nature aging

Article

https://doi.org/10.1038/s43587-022-00309-6

Sphingolipids accumulate in aged muscle, and their reduction counteracts sarcopenia

Received: 10 November 2020

Accepted: 7 October 2022

Published online: 16 December 2022

Check for updates

Pirkka-Pekka Laurila[1,17] ✉, Martin Wohlwend[1,17], Tanes Imamura de Lima[1], Peiling Luan[1], Sébastien Herzig[1], Nadège Zanou[2], Barbara Crisol[1], Maroun Bou-Sleiman[1], Eleonora Porcu[3,4], Hector Gallart-Ayala[5], Michal K. Handzlik[6], Qi Wang[1], Suresh Jain[7], Davide D'Amico[1], Minna Salonen[8], Christian M. Metallo[6], Zoltan Kutalik[3,9], Thomas O. Eichmann[10,11], Nicolas Place[2], Julijana Ivanisevic[5], Jari Lahti[12,13], Johan G. Eriksson[14,15,16] & Johan Auwerx[1] ✉

Age-related muscle dysfunction and sarcopenia are major causes of physical incapacitation in older adults and currently lack viable treatment strategies. Here we find that sphingolipids accumulate in mouse skeletal muscle upon aging and that both genetic and pharmacological inhibition of sphingolipid synthesis prevent age-related decline in muscle mass while enhancing strength and exercise capacity. Inhibition of sphingolipid synthesis confers increased myogenic potential and promotes protein synthesis. Within the sphingolipid pathway, we show that accumulation of dihydroceramides is the culprit disturbing myofibrillar homeostasis. The relevance of sphingolipid pathways in human aging is demonstrated in two cohorts, the UK Biobank and Helsinki Birth Cohort Study in which gene expression-reducing variants of *SPTLC1* and *DEGS1* are associated with improved and reduced fitness of older individuals, respectively. These findings identify sphingolipid synthesis inhibition as an attractive therapeutic strategy for age-related sarcopenia and co-occurring pathologies.

Healthy aging, defined as "freedom from disease, high cognitive and physical functioning, and active engagement with life[1]," will remain the major goal of the public health sector due to the aging of the population, with the proportion of individuals aged 60 years or older expected to rise to 22% in the next four decades[2]. This goal is encumbered by multimorbidity, the coexistence of two or more chronic conditions such as diabetes and cardiovascular and neurodegenerative diseases, whose prevalence is increased upon aging[3]. During the course of these diseases, there is a marked rise in the incidence of a common debilitating comorbidity, age-associated muscle dysfunction.

[1]Laboratory of Integrative Systems Physiology, École polytechnique fédérale de Lausanne (EPFL), Lausanne, Switzerland. [2]Institute of Sport Sciences and Department of Biomedical Sciences, University of Lausanne, Lausanne, Switzerland. [3]Swiss Institute of Bioinformatics, Lausanne, Switzerland. [4]Center for Integrative Genomics, University of Lausanne, Lausanne, Switzerland. [5]Metabolomics Platform, Faculty of Biology and Medicine, University of Lausanne, Lausanne, Switzerland. [6]Molecular and Cellular Biology Laboratory, The Salk Institute for Biological Studies, La Jolla, CA, USA. [7]Intonation Research Laboratories, Secunderabad, India. [8]Chronic Disease Prevention Unit, National Institute for Health and Welfare, Helsinki, Finland. [9]University Center for Primary Care and Public Health, University of Lausanne, Lausanne, Switzerland. [10]Institute of Molecular Biosciences, University of Graz, Graz, Austria. [11]Center for Explorative Lipidomics, BioTechMed-Graz, Graz, Austria. [12]Department of Psychology and Logopedics, University of Helsinki, Helsinki, Finland. [13]Turku Institute for Advanced Studies, University of Turku, Turku, Finland. [14]Department of General Practice and Primary Health Care, University of Helsinki and Helsinki University Hospital, University of Helsinki, Helsinki, Finland. [15]Folkhälsan Research Center, University of Helsinki, Helsinki, Finland. [16]Department of Obstetrics and Gynecology, National University Singapore, Yong Loo Lin School of Medicine, Singapore, Singapore. [17]These authors contributed equally: Pirkka-Pekka Laurila, Martin Wohlwend. ✉e-mail: pirkka-pekka.laurila@helsinki.fi; admin.auwerx@epfl.ch

During aging, skeletal muscle becomes more dysfunctional, and the reduction of skeletal muscle mass is one of the most important causes of functional decline and loss of independence in aged individuals[4]. Skeletal muscle dysfunction is considered a component of the frailty syndrome[4], an even more accurate predictor of all-cause mortality than age alone[5]. Pre-sarcopenia is characterized by low muscle mass, sarcopenia is characterized by low muscle strength or low physical performance in addition to low muscle mass, and severe sarcopenia encompasses all three criteria[4]. The loss of muscle mass in aging has been thought to arise from a blunted synthetic response to feeding and exercise[6]. In addition, upon aging, skeletal muscle becomes depleted of muscle stem cells (MuSCs)[7], and muscle regeneration is impaired[8]. There is both a quantitative and qualitative decline in MuSCs in aged muscle. MuSCs are sensitive to external stimuli, such as inflammatory agents and local growth factors, which are increased in sarcopenia[9]. Molecularly, these effects can be mediated by transforming growth factor β and Wnt signaling that inhibit the Notch pathway, which is critical for MuSC activation. However, the exact mechanism and the ultimate contribution of MuSCs to sarcopenia remain to be established. Other triggers of age-related muscle dysfunction are thought to include mitochondrial abnormalities, hormonal changes, loss of neuromuscular junctions and activation of inflammatory pathways[4]. More in-depth coverage of the pathogenesis[10] and clinical aspects of sarcopenia[4] can be found in published reviews.

Several pharmacological approaches have been proposed to slow the functional impairment of skeletal muscles, such as treatment with sex hormones, including testosterone, and growth hormones, but because the results from these trials have been variable with only marginal effectiveness[11], there is an urgent need for new therapeutic strategies. As patients with age-related muscle dysfunction frequently have multiple comorbidities[12] and take several medications[13], optimal treatment strategies for sarcopenia would also be effective on coexisting conditions to reduce the burden of polypharmacy.

Sphingolipids are bioactive lipids participating in diverse cellular functions such as inflammation, proliferation, cell growth and cell death[14,15]. Ceramides serve as the hub of sphingolipid metabolism and were among the first sphingolipids to have their bioactive role characterized[14]. Increased ceramide levels have been implicated in many complex diseases, including cardiovascular disease[16], diabetes[17] and Alzheimer's disease[18]. We also showed that ceramide levels are upregulated in human muscular dystrophies, especially Duchenne muscular dystrophy, and that inhibition of sphingolipid biosynthesis can alleviate the symptoms of these dystrophies[19]. In recent years, attention has increasingly focused on inhibiting ceramide generation in vivo to combat metabolic disease[20,21]. Ceramides are also implicated in cellular senescence by activating the p21 pathway[22]. Inhibition of serine–palmitoyl transferase (SPT), the first and rate-limiting enzyme of the sphingolipid de novo biosynthesis pathway, leads to reduced atherosclerosis[23], improved glucose tolerance[24] and fatty liver[25] in mouse models. Mice deficient for ceramide synthase 6 (CERS6) are protected from glucose intolerance[26,27], certain ceramide synthases are correlated with age[28] and the inhibition of dihydroceramide desaturase (DEGS1) was recently reported to improve glucose homeostasis and liver fat accumulation[29]. Sphingolipid metabolism is also implicated in cancer cachexia[30] and apoptosis of myotubes[31]. The increased nuclear factor κB signaling in aging is thought to involve ceramides[32]. While the emerging role of sphingolipid depletion in the treatment of metabolic disorders has been under intensified research efforts[20,21] with pharmacological inhibition of CERS1 observed to produce beneficial effects[33], the hypothesis that inhibition of sphingolipid synthesis could counteract age-related muscle dysfunction, despite its frequent co-occurrence with metabolic disease, has remained unproven.

In the present study, we establish a link between sphingolipid metabolism and age-related loss in muscle mass and function. We show that ceramides accumulate in skeletal muscle upon aging and that genetic and pharmacological inhibition of the sphingolipid de novo biosynthesis pathway counteracts age-related loss in muscle mass and function in aged mice. Systemic inhibition of sphingolipid synthesis activates the myogenic differentiation program in a cell-autonomous manner in muscle progenitor cells, coupled with elevated myocellular protein synthesis. By comprehensive silencing of the members of the sphingolipid de novo synthesis pathway, we show that dihydroceramide accumulation blunts myogenic differentiation. We furthermore demonstrate the relevance of sphingolipid synthesis in human aging by showing that genetic variants of SPT and DEGS1 are associated with fitness and muscle function in older individuals. Our findings implicate sphingolipid de novo biosynthesis inhibition as a new therapeutic strategy for age-associated sarcopenia. Given the diverse cellular functions of ceramides and involvement in multiple diseases[14], treatment of many diseases by targeting only one biological pathway presents an attractive therapeutic strategy to combat age-related multimorbidity.

Results

Ceramides accumulate in skeletal muscle upon aging

The sphingolipid de novo synthesis pathway produces ceramides and other sphingolipids by using fatty acids and amino acids as substrates (Fig. 1a). SPT converts L-serine and palmitoyl–coenzyme A (CoA) to 3-ketosphinganine, which is rapidly converted to sphinganine. Coupling of sphinganine to long-chain fatty acid is accomplished by one of six distinct mammalian ceramide synthases. To study how aging affects the sphingolipid de novo synthesis pathway in vivo, we compared total ceramide content of different organs in young (2-month-old) and aged (2-year-old) mice. Upon aging, we observed a decrease of ceramide levels in the liver and brain and an increase in skeletal muscle (Fig. 1b and Supplementary Fig. 1a–d). Sphingomyelin levels in different organs reflected their respective ceramide profiles, yet were less pronounced (Supplementary Fig. 1e–h). The profile of plasma ceramides and sphingomyelins closely mirrored that of the liver (Supplementary Fig. 1d,h). Given that the effects of modulating ceramide quantity and quality in liver are established[29,34], we here focused on skeletal muscle sphingolipids and potential benefits following their reduction.

The trend of age-dependent increase in skeletal muscle ceramides was global, comprising ceramide species with different acyl lengths (Fig. 1c). The most pronounced increase upon aging was observed for Cer(d18:1/24:1) (Fig. 1c). Differences in skeletal muscle sphingomyelin, a sphingolipid consisting of phosphocholine and ceramide, were less consistent between young and aged mice (Supplementary Fig. 1e). Deoxysphingolipids are synthesized by SPT through conjugation of L-alanine rather than L-serine with fatty acid and have been implicated in disease conditions, such as diabetes[35]. Similarly to canonical sphingolipids, there was a trend of deoxysphinganine (doxSA) accumulation in skeletal muscle upon aging (Supplementary Fig. 2a).

We next compared the transcript abundance of the enzymes of the sphingolipid de novo biosynthesis pathway between young and older human individuals in a publicly available dataset (GSE25941). Consistent with increased muscle ceramides, many transcripts of these enzymes were upregulated upon aging, including *SPTLC1*, *KDSR*, *CERS2* and *CERS5* (Fig. 1d). The only downregulated enzyme was *CERS1* (Fig. 1d). Analysis of the human skeletal muscle transcript profile of postmortem biopsies from the Genotype-Tissue Expression (GTEx) dataset ($n = 491$) revealed a strong positive correlation between different transcripts of the sphingolipid de novo biosynthesis pathway (Fig. 1e). Again, only *CERS1* transcripts displayed a negative correlation with the other enzymes. Similarly, in the mouse BXD strains[36], a recombinant inbred mouse population with substantial genetic heterogeneity, the transcripts were directly correlated with each other (Fig. 1f). These results suggest that the sphingolipid de novo biosynthesis pathway is under tightly coordinated transcriptional control.

https://doi.org/10.1038/s43587-022-00309-6

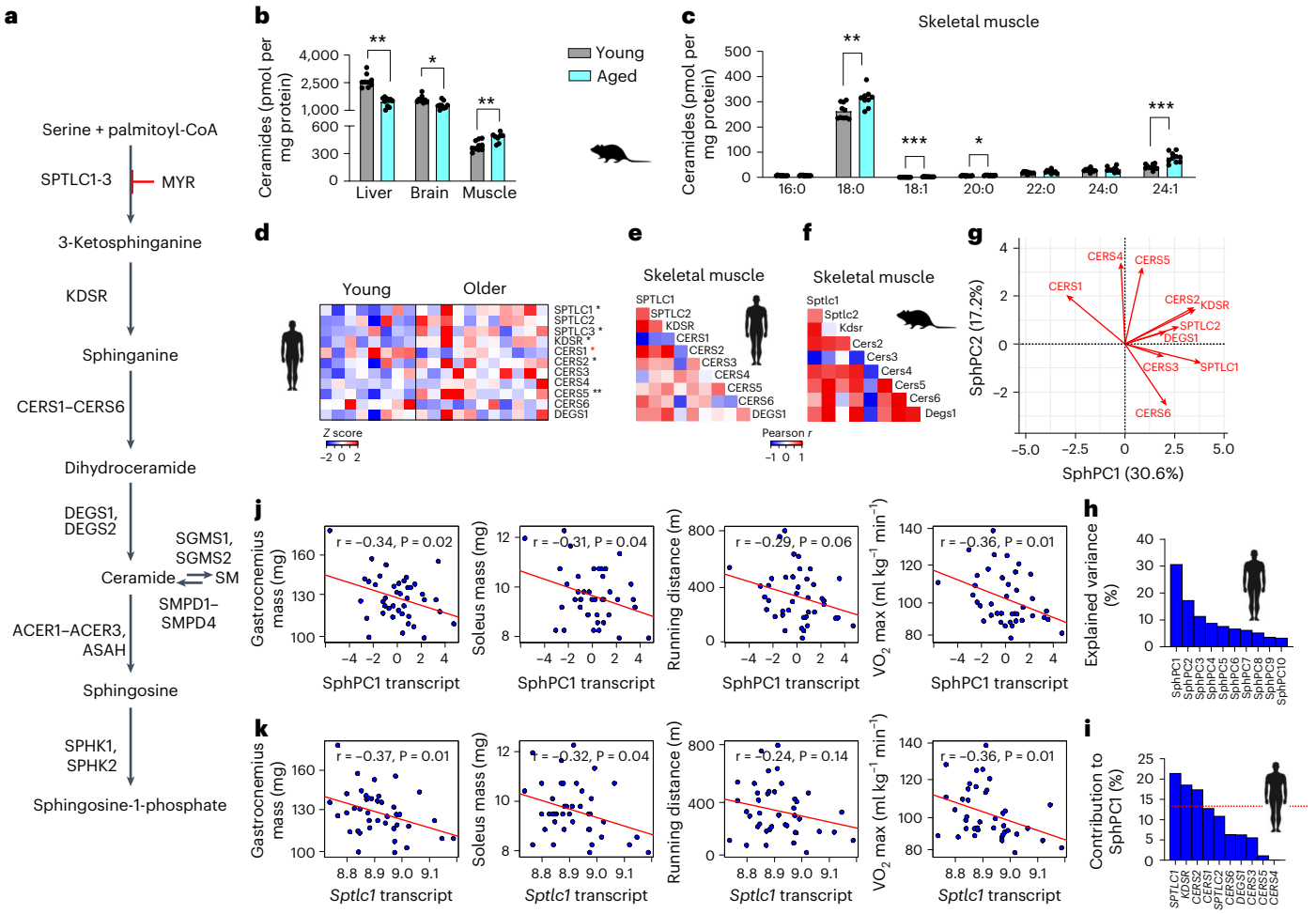

Fig. 1 | Sphingolipid de novo synthesis is activated upon aging in skeletal muscle. a, Schematic of the sphingolipid de novo synthesis pathway. SM, sphingomyelin. **b**, Total ceramide levels in the liver, brain, skeletal muscle and plasma of young (8-week-old, $n = 10$) and aged (24-month-old, $n = 10$) C57BL/6JRj mice. **c**, Concentrations of individual ceramide species in mouse quadriceps muscle. **d**, Transcript abundance of enzymes of the sphingolipid de novo synthesis pathway in the skeletal muscle of young and older human individuals (GSE25941). **e**, Correlation of transcripts of the sphingolipid de novo synthesis pathway in human skeletal muscle (GTEx, $n = 491$). **f**, Correlation of transcripts of the sphingolipid de novo synthesis pathway in the skeletal muscle of 42 genetically diverse BXD strains. **g**, A factor loading plot (biplot) showing the effects of the enzymes of the sphingolipid de novo synthesis pathway on the first two principal components (SphPC1 and SphPC2) in human skeletal muscle (GTEx). **h**, Proportion of variance explained by each principal component of the sphingolipid de novo synthesis pathway. **i**, Contribution of each transcript to the SphPC1 in human skeletal muscle (GTEx). **j**, Pearson correlation of SphPC1 in the skeletal muscle with measurements of muscle mass and function in BXD mice. VO_2 max (maximal oxygen consumption). **k**, Pearson correlation of *Sptlc1* in the skeletal muscle with measurements of muscle mass and function in BXD mice. Student's two-tailed *t*-test with Benjamini–Hochberg (BH) adjustment for false discovery rate (FDR). All data are shown as mean ± s.e.m. *, BH FDR < 0.05; **, BH FDR < 0.01; and ***, BH FDR < 0.001. Icon credits: humans, FreeVectors.net; mouse, clipart.com.

As there was a strong correlation between transcripts of the pathway in skeletal muscle, we performed principal-component analysis of the sphingolipid de novo biosynthesis pathway in humans (Fig. 1g) and mice (Supplementary Fig. 2b–d). Of the variation in expression in the skeletal muscle sphingolipid de novo synthesis pathway, the first principal component of the sphingolipid de novo synthesis pathway (abbreviated here as 'SphPC1') explained 30.6% (Fig. 1h), and *SPTLC1* contributed the most to the variability in humans, accounting for 21% (Fig. 1i). In the BXD mouse reference population, we observed negative correlation between SphPC1 and both gastrocnemius and soleus muscle masses, as well as performance on a treadmill and maximal aerobic capacity (Fig. 1j). The expression of *Sptlc1* in skeletal muscle showed similar correlations with these phenotypes (Fig. 1k). These findings demonstrate that the expression of components of the sphingolipid de novo biosynthesis pathway is inversely correlated with muscle mass and function and suggest involvement of this pathway in age-related muscle dysfunction.

Reduction of sphingolipids prevents loss of muscle mass and function in aging

To examine whether inhibition of the sphingolipid de novo biosynthesis pathway could protect against age-related muscle dysfunction, we treated aged (18-month-old) chow-fed C57BL/6JRj male mice for 6 months with myriocin, an inhibitor of SPT, the first and rate-limiting enzyme of the sphingolipid de novo synthesis pathway and whose expression in skeletal muscle was negatively correlated with muscular fitness in BXD mice (Fig. 1k). Myriocin treatment reduced the total ceramide content of skeletal muscle (Fig. 2a) as well as that of individual ceramide species in a global fashion in aged mice (Fig. 2b and Supplementary Fig. 2e,f), confirming the desired effect of the compound in the skeletal muscle. This was further confirmed by high-performance liquid chromatography (HPLC)–tandem mass spectrometry showing that myriocin penetrated skeletal muscle (Supplementary Fig. 3a). In addition to ceramides, myriocin reduced skeletal muscle deoxysphingolipid

https://doi.org/10.1038/s43587-022-00309-6

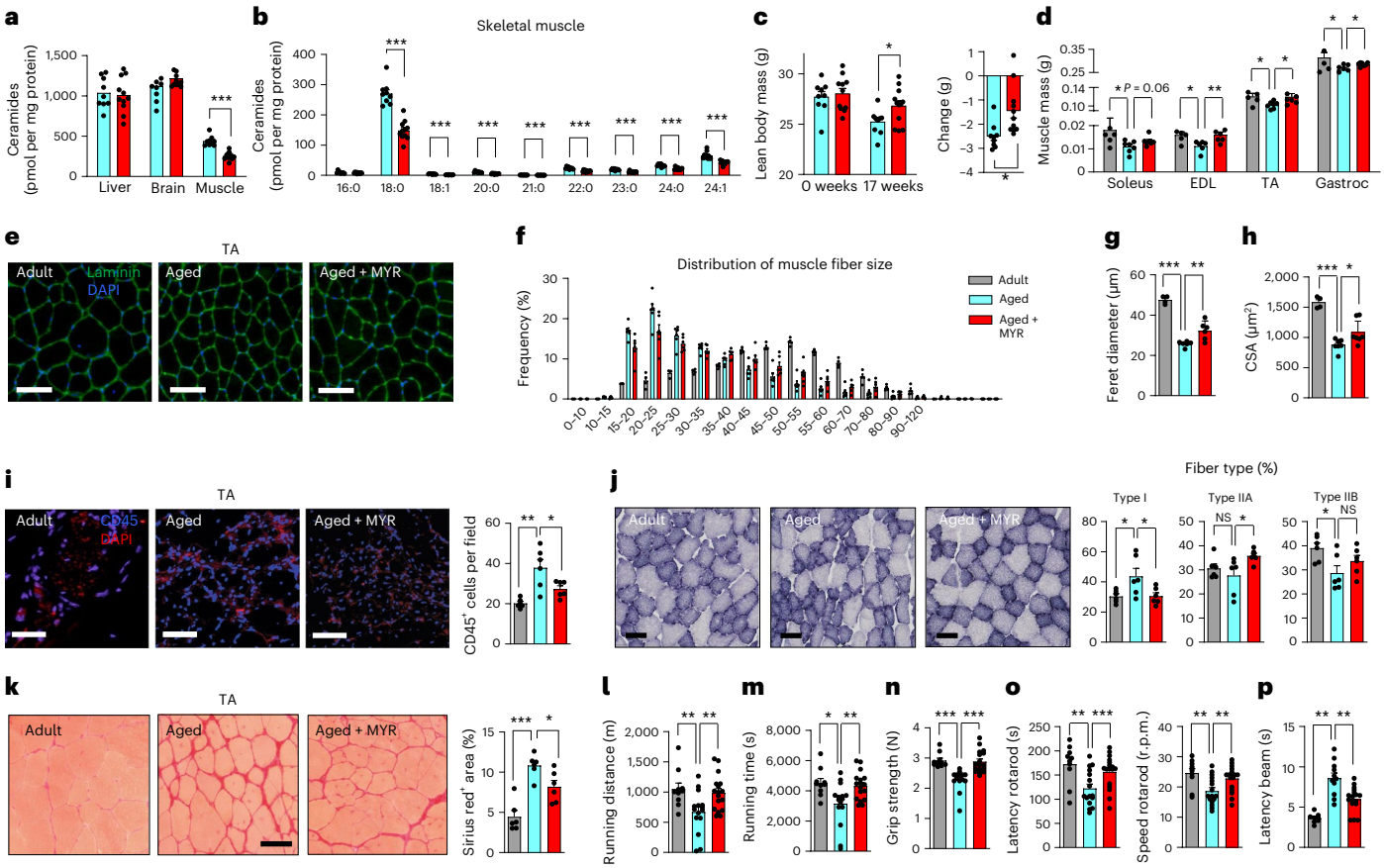

Fig. 2 | Inactivation of sphingolipid de novo synthesis increases muscle mass and improves muscle function. Aged (18-month-old) C57BL/6JRj mice were treated with intraperitoneal injections of myriocin (MYR) for 5 months at 0.4 mg kg^{-1} 3 times per week. **a**, Total ceramide levels. **b**, Concentrations of individual ceramide species in mouse quadriceps muscle. **c**, Lean body mass measured before and after treatment and its change. **d**, Soleus, EDL, gastrocnemius and TA mass. For **a**–**d**, young mice, $n = 6$; aged mice, $n = 9$; aged mice + MYR, $n = 11$. **e**, Representative images of laminin staining of TA muscle in young mice, aged mice and aged mice treated with myriocin. Scale bars, 50 µm. **f**–**h**, Distribution of muscle fiber size (**f**), mean of fiber minimal Feret diameter (**g**) and CSA (**h**) in TA muscle. **i**–**k**, Representative images and quantification of CD45 immunostaining (**i**), SDH staining (**j**) and Sirius red staining (**k**) in TA muscle. Scale bars, 50 µm. For **f**–**k**, aged mice, $n = 6$; aged mice + MYR, $n = 6$. **l**–**p**, Comparison of maximal running distance and duration ($n = 10$, 15 and 17) (**l**–**m**), grip strength ($n = 10$, 14 and 17) (**n**), latency and maximal speed on the rotarod test ($n = 10$, 16 and 17) (**o**) and latency of beam crossing ($n = 8$, 11 and 17) (**p**) between aged DMSO- and MYR-treated mice. Student's two-tailed *t*-test with BH adjustment for FDR. All data are shown as mean ± s.e.m. *, BH FDR < 0.05; **, BH FDR < 0.01; and ***, BH FDR < 0.001. NS, non-significant.

content, yet with a smaller effect than for L-serine-derived canonical sphingolipids (Supplementary Fig. 2a). Myriocin did not induce hepatoxicity in aged mice, as measured by the liver enzymes alanine transaminase and aspartate transaminase (Supplementary Fig. 2g,h), indicating that myriocin is well tolerated by aged mice.

Importantly, myriocin improved the body composition of aged mice. Myriocin delayed the age-dependent decline in lean body mass (Fig. 2c) and increased muscle mass. Myriocin-treated mice displayed greater skeletal muscle weight (extensor digitorum longus (EDL), soleus, gastrocnemius and tibialis anterior (TA)) mass than dimethyl sulfoxide (DMSO)-treated controls (Fig. 2d). While the fiber size was reduced in aged mice as compared to adult mice, myriocin improved the morphology in histological analyses of TA muscles, as manifested by larger cross-sectional area (CSA) of muscle fibers (Fig. 2e–h). In addition, myriocin reduced age-induced inflammation in skeletal muscle, as observed by reduced CD45 (Fig. 2i) and F4/80 (Supplementary Fig. 3b) positivity in skeletal muscle staining. Aging is associated with loss of fast-twitch type II muscle fibers[37], and maintenance of fast-twitch fibers in aging has been shown to be beneficial in sarcopenia[38]. Myriocin kept the fiber type profile closer to that of younger mice (Fig. 2j). Importantly, myriocin protected against age-induced fibrosis in skeletal muscle as reflected by Sirius red staining (Fig. 2k).

Myriocin also counteracted age-related muscle dysfunction. Aged mice treated with myriocin demonstrated improved exercise performance and muscle strength, as evidenced by increased running distance and time on a treadmill (Fig. 2l,m) and grip strength (Fig. 2n). Myriocin-treated mice also displayed better muscle coordination, as shown by their improved performance in the rotarod test (Fig. 2o) and faster crossing of a beam (Fig. 2p). Overall, myriocin treatment improved muscle morphology and counteracted age-related loss of muscle mass, strength, endurance and coordination, indicating protection against age-relaed muscle dysfunction.

To identify biological pathways whose modulation could explain improved muscle function in aging upon myriocin treatment, we compared the transcriptomes of the quadriceps muscle of aged myriocin- and DMSO-treated mice using RNA sequencing. We performed gene set enrichment analysis (GSEA) ranking the transcripts based on their fold change. The pathways most downregulated by myriocin treatment were related to the extensively studied role of sphingolipids in lipid metabolism and inflammation, while upregulated pathways were related to muscle contraction and differentiation (Fig. 3a,b and

https://doi.org/10.1038/s43587-022-00309-6

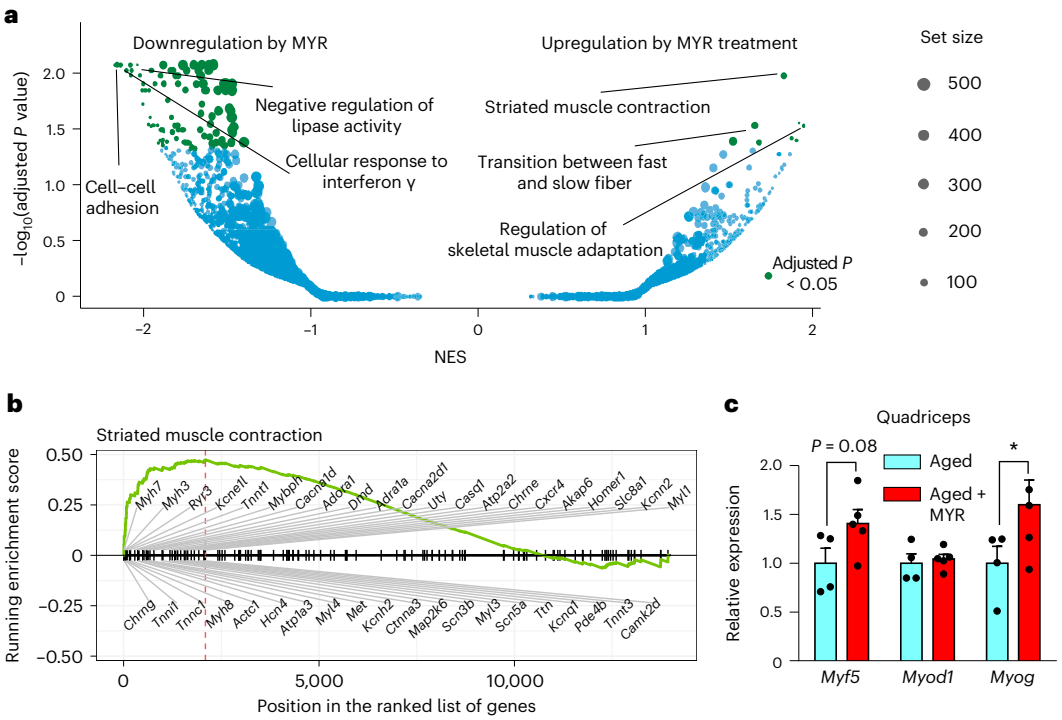

Fig. 3 | Inhibition of sphingolipid de novo synthesis transcriptionally upregulates myogenic differentiation. a, Volcano plot of the gene sets (Gene Ontology (GO) categories) with normalized enrichment score (NES) and adjusted *P* value, as described in ref. [79], for each gene set given. **b**, Enrichment plot of the 'striated muscle contraction', the most upregulated GO category by MYR. **c**, Comparison of transcripts of *Myf5*, *Myod1* and *Myog* in aged mice and aged mice treated with MYR as described in Fig. 2. For **a**–**c**, aged mice, $n = 4$; aged mice + MYR, $n = 5$. Student's two-tailed *t*-test with BH adjustment for FDR. All data are shown as mean ± s.e.m. *, BH FDR < 0.05; **, BH FDR < 0.01; and ***, BH FDR < 0.001.

Supplementary Fig. 4a–c). Indeed, in a targeted analysis of canonical transcription factors governing myogenesis, *Myog* and *Myf5* were upregulated in skeletal muscle upon myriocin treatment (Fig. 3c), in line with the reported effects of sphingolipids on rat myoblasts[39].

SPT inactivation in muscle improves age-related fitness

Inhibition of the sphingolipid de novo synthesis pathway has previously been linked to systemic effects, including improved insulin sensitivity[24,29], which might affect muscle function. To study the muscle-specific role of *Sptlc1* inhibition, we silenced *Sptlc1* in gastrocnemius muscles in aged (18-month-old) male C57BL/6JRj mice using adeno-associated virus (AAV) serotype 9 intramuscular injection (Fig. 4a). Phenotypic tests were performed 6 months after the AAV injections. Silencing of *Sptlc1* in gastrocnemius of aged mice resulted in improved performance in tests measuring uphill running (Fig. 4b) and grip strength (Fig. 4c). Similarly to myriocin treatment, both gastrocnemius mass and muscle CSA were increased in aged mice with AAV-mediated inactivation of *Sptlc1* in gastrocnemius (Fig. 4d,e). Importantly, gastrocnemius muscles in which *Sptlc1* expression was silenced using AAVs were more resistant to age-related fibrosis (Fig. 4f). Transcripts involved in the myogenic differentiation pathway were induced in gastrocnemius, reminiscent of the changes seen upon systemic myriocin treatment in aged mice (Fig. 4g). Furthermore, ceramide levels were decreased in aged gastrocnemius muscles following AAV treatment (Fig. 4h). Thus, our findings demonstrate that skeletal muscle-specific genetic inactivation of *Sptlc1* also improves muscle morphology and function in aging.

SPT inactivation promotes myogenesis and protein synthesis

To study whether sphingolipid depletion has a cell-autonomous effect on muscle differentiation, we isolated primary MuSCs from aged mice. Myogenic differentiation involves MuSCs, which are capable of giving rise to mature muscle fibers, and their regenerative capacity has been reported to be impaired upon aging[40]. When incubating freshly isolated MuSCs in myriocin-containing medium, we observed elevation of MYOD and MYOG protein levels (Fig. 5a,b), indicating that inhibition of sphingolipid synthesis cell autonomously primes MuSCs for myogenic differentiation. We also verified that the myogenic ability conferred by myriocin does not deplete the MuSC pool of aged mice. In line with previous reports[7,41], we observed a decrease in MuSC count upon aging, but relative to DMSO-treated mice, myriocin prevented this reduction (Fig. 5c–e).

Myofibrillar protein synthesis is required to produce mature myofibers, which are the outcome of myogenic differentiation. To assess whether inhibition of sphingolipid de novo synthesis promotes protein synthesis in the myogenic lineage, we measured puromycin incorporation, a measure of protein synthesis rate, in myriocin-treated C2C12 myogenic progenitors. In line with increased levels of muscle differentiation markers in MuSCs (see above), we observed elevated levels of puromycin incorporation upon myriocin treatment (Fig. 5f). To further investigate the underlying mechanism by which myriocin promotes protein synthesis in C2C12 myogenic progenitors, we assessed pathways associated with protein translation and degradation. Western blot data showed reduced levels of muscle RING-finger protein-1 (MuRF) upon myriocin treatment (Fig. 5g,h), suggesting that sphingolipid inhibition reduces muscle protein degradation. Moreover, phosphorylation levels of p70S6K and 4E-BP1 were increased upon myriocin treatment (Fig. 5g,h), pointing toward enhanced protein synthesis when sphingolipid synthesis is blocked. We used a concentration of 30 µM of myriocin for experiments in Fig. 5; however, our subsequent experiments show that a nanomolar concentration of myriocin is enough to produce similar effects. Together, these results indicate that myriocin promotes myogenic progenitor differentiation and protein synthesis by activating protein translation and inactivating protein degradation in a cell-autonomous fashion.

https://doi.org/10.1038/s43587-022-00309-6

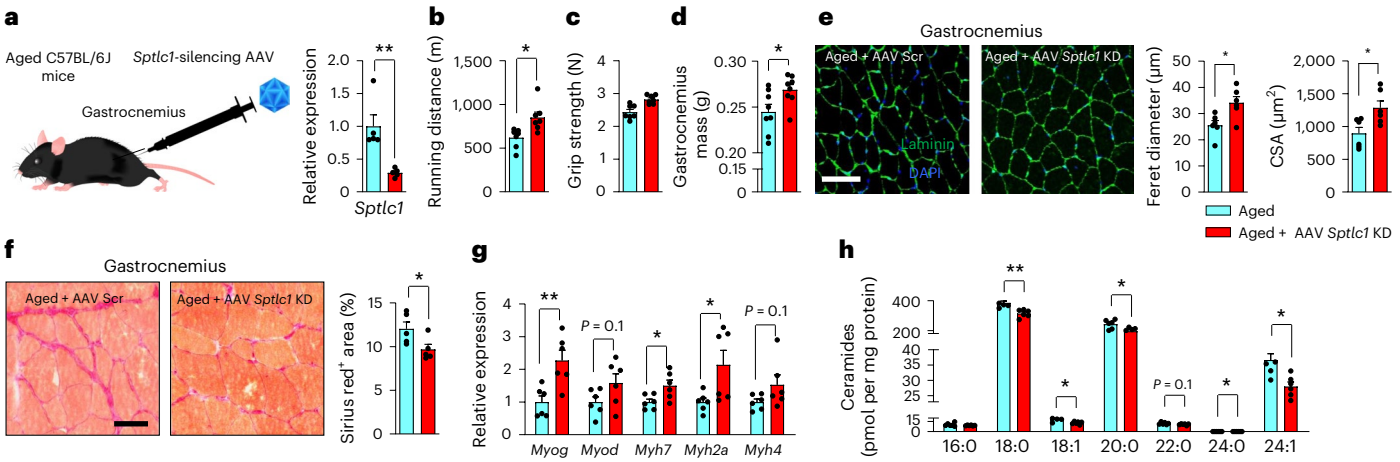

Fig. 4 | Skeletal muscle-specific *Sptlc1* inhibition improves muscle morphology and function in aged mice. a, Schematic showing bilateral gastrocnemius injections of AAV9 particles containing scrambled (aged + Scr) or *Sptlc1*-targeting (aged + AAV *Sptlc1* KD) short hairpin RNA in 18-month-old C57BL/6JRj mice and validation of *Sptlc1* knockdown in gastrocnemius muscle using qPCR. Phenotyping, histology and biochemical assays were assessed in 24-month-old mice, 6 months after AAV9 injections. For (**b**–**h**), aged control animals are compared to *Sptlc1* knockdown mice. **b**, Maximal running distance ($n = 8$ per group). **c**, Grip strength ($n = 8$ per group). **d**, Gastrocnemius muscle mass ($n = 8$ per group). **e**, Representative images of laminin immunostaining of gastrocnemius muscle with quantification of minimal Feret diameter and CSA. Scale bar, 50 μm ($n = 5$ per group). **f**, Representative gastrocnemius histology staining for Sirius red and quantification of fibrosis area. Scale bar, 50 μm ($n = 5$ per group). **g**, Normalized quantitative RT–PCR in mouse gastrocnemius muscle ($n = 6$ per group). **h**, Concentrations of individual ceramide species in mouse gastrocnemius muscle ($n = 6$ per group). Student's two-tailed *t*-test with BH adjustment for FDR. All data are shown as mean ± s.e.m. *, BH FDR < 0.05; **, BH FDR < 0.01; and ***, BH FDR < 0.001. Image credits: mouse, Vecteezy.com; syringe, Pixabay.com; icosahedron, Shutterstock.com.

Sptlc1 and *Cers2* inactivation enhances myogenic differentiation

As the sphingolipid de novo synthesis pathway consists of multiple enzymatic conversions of substrates to their products (Fig. 1a), inhibition of sphingolipid de novo synthesis results in the reduction of a number of lipid species downstream of SPT, not only ceramides. To identify the sphingolipid species responsible for the effect on myogenic differentiation, we silenced enzymes of the sphingolipid de novo synthesis pathway in a systematic manner using CRISPR–Cas9 in C2C12 myoblasts.

Incubation of C2C12 myoblasts with myriocin reduced ceramide and dihydroceramide levels (Fig. 6a,b and Supplementary Fig. 5a,b) and accelerated myoblast differentiation (Fig. 6c), as shown by a greater fusion index (Fig. 6d) and myotube area (Fig. 6e), and induced a myogenic transcript signature featuring upregulation of myogenic transcription factors, such as *Myog*, as well as markers of mature myotubes, including myosin heavy chain subunits *Myh4* and *Myh1* (Fig. 6f). In addition to myriocin, we tested another SPT inhibitor, termed Takeda 2 (refs.[42,43]). Similarly to myriocin, Takeda 2 enhanced myogenesis as demonstrated by greater myotube fusion index and area, as well as transcript markers of myogenesis, and reduced sphingolipid levels (Supplementary Fig. 6a–f).

To confirm that genetic ablation of SPT could induce similar effects as myriocin, we generated polyclonal knockouts (KOs) of *Sptlc1* using CRISPR–Cas9 in C2C12 myoblasts. Silencing of *Sptlc1* ($Sptlc1^{KO}$) reduced levels of ceramides and dihydroceramides (Fig. 6g,h and Supplementary Fig. 5c,d) and promoted myoblast differentiation (Fig. 6i), as determined by quantification of fusion index (Fig. 6j), myotube area (Fig. 6k) and a myogenic transcript signature similar to MYR-treated cells (Fig. 6l). In addition to the polyclonal $Sptlc1^{KO}$ cells, we generated monoclonal $Sptlc1^{KO}$ cells. Using CRISPR–Cas9 genome editing, we were able to obtain both homozygous ($Sptlc1^{-/-}$) and heterozygous ($Sptlc1^{+/-}$) knockout lines (Supplementary Fig. 7a–c). These knockouts promoted myogenesis in an allele dose-dependent manner, with $Sptlc1^{-/-}$ myoblasts displaying greater myotube area than $Sptlc1^{+/-}$ or empty vector cells (Supplementary Fig. 7d–g), indicating that SPT abundance dose dependently influences muscle differentiation.

We also silenced *Cers2* ($Cers2^{KO}$), the most abundant ceramide synthase in skeletal muscle, downstream of SPT. Inactivation of *Cers2* reduced the levels of very-long-chain (C20–C24) dihydroceramides and ceramides (Fig. 6m,n and Supplementary Fig. 5e,f) and led to accelerated myogenesis (Fig. 6o–q), featuring a similar gene expression signature (Fig. 6r) to that observed after myriocin treatment.

In contrast to its upstream counterparts, inactivation of *Degs1* ($Degs1^{KO}$), the subsequent component of the pathway, while reducing ceramide levels, caused an accumulation of dihydroceramides (Fig. 6s,t and Supplementary Fig. 5g,h). Instead of promoting myogenic differentiation, inactivation of *Degs1* inhibited myoblast differentiation (Fig. 6u) observed as reduction in fusion index (Fig. 6v,w) as well as downregulation of markers of mature myotubes (Fig. 6x), suggesting that accumulation of dihydroceramides could impair myogenic differentiation.

To further investigate the effects of dihydroceramides in skeletal muscle cells, we silenced the two subunits of sphingomyelin synthase (SMS), an enzyme converting ceramides to sphingomyelins or dihydroceramides to dihydrosphingomyelin (DHSM), using small interfering RNAs, in addition to CRISPR-Cas9-mediated knockdown of *Degs1* (Supplementary Fig. 8a). The single $Degs1^{KO}$ and the triple knockout of *Degs1*, *Sgms1* and *Sgms2* reduced ceramide contents (Supplementary Fig. S8b), and as expected, $Degs1^{KO}$ cells displayed higher dihydroceramide content compared to control myoblasts, which was further elevated by triple silencing of *Degs1*, *Sgms1* and *Sgms2* (Supplementary Fig. 8c). Inhibition of myoblast differentiation was observed again in $Degs1^{KO}$ myoblasts (Supplementary Fig. 8d), as measured by fusion index (Supplementary Fig. 8e), myotube area (Supplementary Fig. 8f) and transcript markers of myogenic differentiation (Supplementary Fig. 8g). Notably, co-silencing of *Degs1* together with *Sgms1* and *Sgms2* further impaired myogenic differentiation (Supplementary Fig. 8d–g). These results suggest that dihydroceramides rather than

https://doi.org/10.1038/s43587-022-00309-6

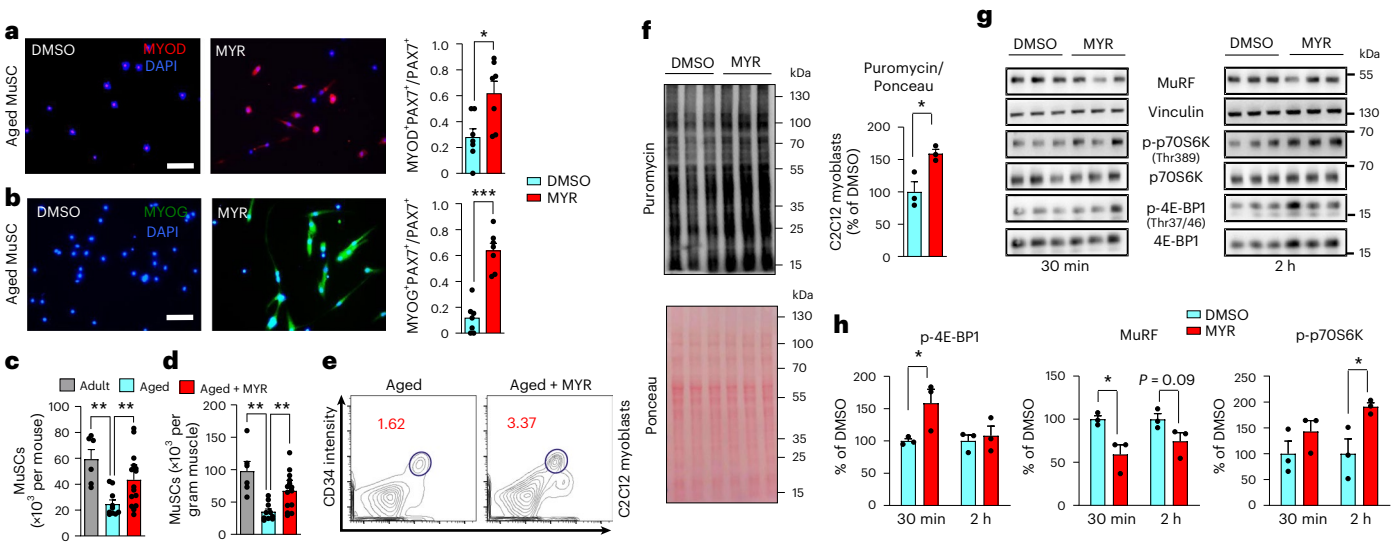

Fig. 5 | Sphingolipid depletion activates myogenic differentiation cell autonomously and promotes protein synthesis. a,**b**, Immunocytochemistry and quantification of MYOD (**a**) and MYOG (**b**) from freshly isolated MuSCs from aged C57BL/6JRj mice after incubation for 72 h in DMSO- or 30 µM MYR-containing medium. Scale bars, 50 µm. For **a**,**b**, $n = 6$ per group. **c**,**d**, Number of freshly isolated MuSCs from the total hindlimbs musculature (**c**) and normalized to muscle weight (**d**) from young mice, aged mice and aged mice treated with MYR. **e**, FACS contour plot of α7 integrin$^+$CD34$^+$Sca-1$^-$CD45$^-$CD31$^-$CD11b$^-$ cells corresponding to MuSCs isolated from aged mice and aged mice treated with MYR. For **c**–**e**, young mice, $n = 6$; aged mice, $n = 10$; aged mice + MYR, $n = 15$. **f**, Puromycin incorporation and quantification of DMSO- and MYR-treated C2C12 myoblasts. **g**,**h**, Western blots (**g**) and quantification (**h**) of markers of protein synthesis and degradation. $n = 3$ per group. Student's two-tailed t-test with BH adjustment for FDR. All data are shown as mean ± s.e.m. *, BH FDR < 0.05; **, BH FDR < 0.01; and ***, BH FDR < 0.001.

dihydrosphingomyelins are responsible for reduction in myogenic differentiation.

Inhibition of *DEGS1* blunts myogenic differentiation

The pathophysiological role of DEGS1 and dihydroceramides is an emerging question in sphingolipid biology[44,45]. The enzyme DEGS1 converts dihydroceramides to ceramides by inserting a Δ4,5$^-$*trans*-double bond to the sphinganine backbone. Previous studies have suggested that dihydroceramides and ceramides might have distinct cellular functions[44,45], and given that *Degs1* silencing, in contrast to that of other upstream enzymes, did not boost myoblast differentiation, we examined whether *Degs1* inhibition could not only inhibit myogenesis, but even abrogate the *Sptlc1* deficiency-induced accelerated myotube formation. As poor aqueous solubility makes exogenous delivery of physiological long-chain sphingolipids difficult[46], we administered GT-11 and sphinganine to myoblasts to load them with dihydroceramides according to a previously described method[47] (Fig. 7a). GT-11 was added to pharmacologically inhibit DEGS1 and sphinganine to ensure substrate availability for dihydroceramide formation in *Sptlc1*-deficient myoblasts.

Consistent with our results above (Fig. 6g–l), *Sptlc1* silencing in C2C12 myoblasts reduced both ceramide and dihydroceramide levels (Fig. 7b,c and Supplementary Fig. 9a,b). Administration of DEGS1 inhibitor GT-11 together with sphinganine to *Sptlc1*-deficient myoblasts further reduced ceramides and increased dihydroceramides (Fig. 7b,c and Supplementary Fig. 9a,b). Again, *Sptlc1* deficiency promoted myogenic differentiation of C2C12 myoblasts, as evidenced by increased fusion index (Fig. 7d), myotube area (Fig. 7e) and a myogenic transcript signature featuring upregulation of both myogenic regulatory factors, including *Myod1*, *Myog* and *Myf6* (Fig. 7f), and muscle contractile proteins (Fig. 7g). Addition of sphinganine and GT-11 abrogated the myogenic effects of *Sptlc1* deficiency (Fig. 7d–h), indicating that both pharmacological and genetic inhibition of the enzyme converting dihydroceramides to ceramides disrupts myogenic differentiation.

To study whether dihydroceramide levels are upregulated upon aging, we measured dihydroceramide concentration in the skeletal muscle of aged C57BL/6JRj mice. Aging increased skeletal muscle dihydroceramide content (Fig. 7i and Supplementary Fig. 9c), which was reduced by myriocin treatment (Fig. 7j and Supplementary Fig. 9d). Thus, dihydroceramides could be involved in muscle aging, while their reduction could be associated with beneficial muscular effects. To explore this, we studied whether genetic variation in *DEGS1* influences age-related fitness in humans.

Genetic evidence of sphingolipid metabolism in human aging

To determine whether sphingolipid depletion could stimulate muscle differentiation in human cell lines, we treated human primary myoblasts with 30 µM myriocin. Consistent with mouse myoblasts, myriocin accelerated human myoblast differentiation, with cells displaying larger myotube area (Fig. 7k,l). Thus, SPT inhibition could enhance muscle maintenance also in human muscles.

We finally investigated whether the sphingolipid de novo synthesis pathway is involved in age-related muscle dysfunction in humans by performing genetic association analyses in older individuals in different studies. Hand grip strength is considered a biomarker of health status in aging[48]. Given that grip strength was measured in participants of the UK Biobank (UKBB) study[49] and that muscle sphingolipid metabolism was linked to fitness phenotypes in mouse models in our study, we performed association analysis of single-nucleotide polymorphisms (SNPs) located within ±150 kb of the *SPTLC1* gene, the target of myriocin, and *DEGS1*, the enzyme converting dihydroceramides to ceramides, with right and left hand grip strength in older (≥ 65 years) UKBB participants ($n = 93{,}211$). Both *SPTLC1* and *DEGS1* regions consist of four haploblocks (Fig. 7m), and within the *SPTLC1* region, we identified rs10820914, a SNP located 140 kb from *SPTLC1*, to be most significantly associated with right ($\beta = 0.94$, $P = 0.001$) and left ($\beta = 0.88$, $P = 0.003$) hand grip strength in UKBB participants (Fig. 7n). In the *DEGS1* region, we identified rs35533869, a SNP located within 110 kb from *DEGS1*, to be most significantly associated with right

https://doi.org/10.1038/s43587-022-00309-6

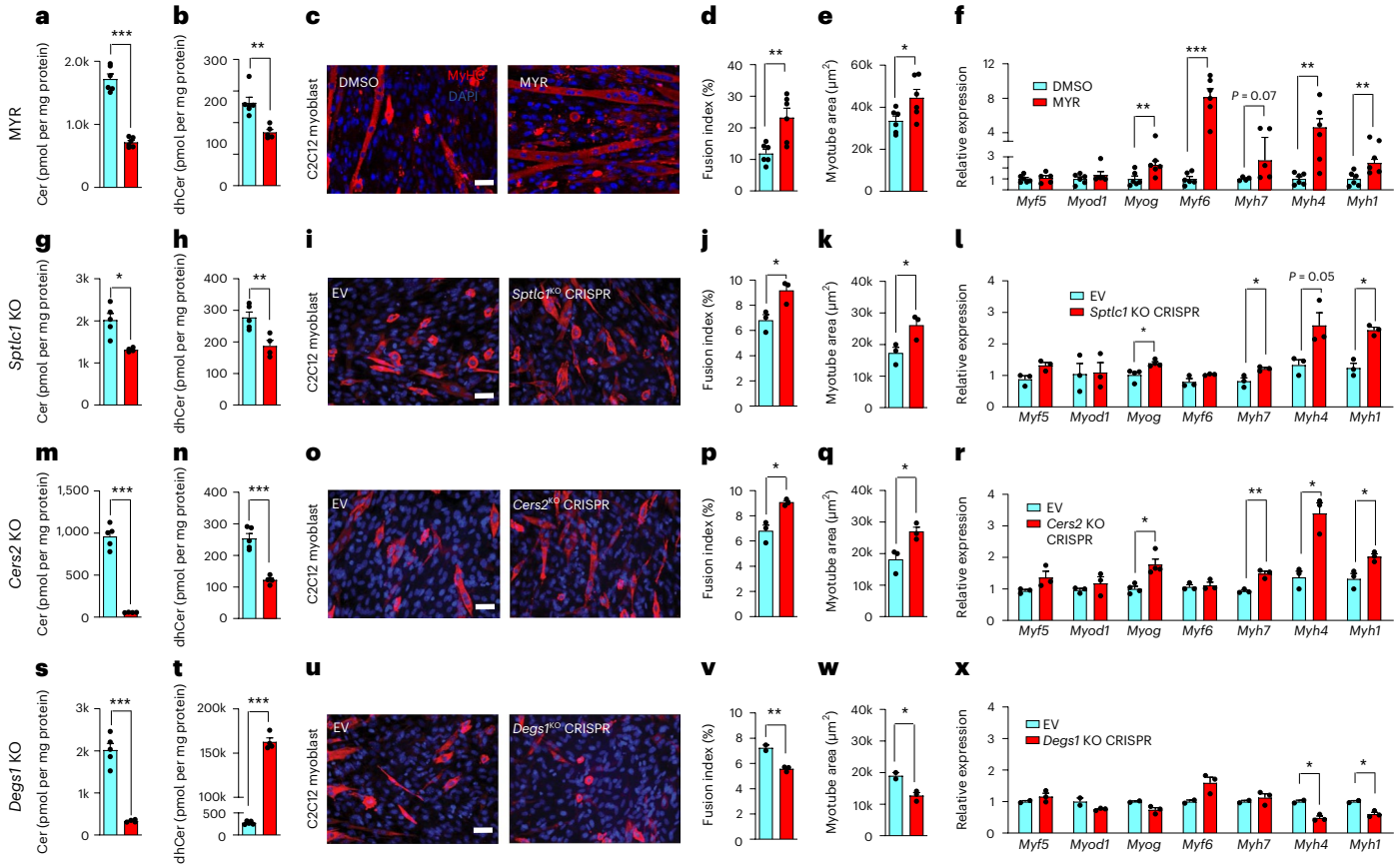

Fig. 6 | Sphingolipid depletion cell autonomously activates muscle differentiation in progenitor cells. a–**f**, Total ceramide (**a**) and dihydroceramide (**b**) levels, immunocytochemistry (**c**), fusion index (**d**), myotube area (**e**) and expression of myogenesis markers (**f**) from C2C12 myoblasts grown in DMSO- or 100 nM MYR-containing medium. **g**–**l**, Total ceramide (**g**) and dihydroceramide (**h**) levels, immunocytochemistry (**i**), fusion index (**j**), myotube area (**k**) and gene expression of myogenesis markers (**l**) from C2C12 *Sptlc1*^{KO} myoblasts. **m**–**r**, Total C20–C24:1 ceramide (**m**) and dihydroceramide (**n**) levels, immunocytochemistry (**o**), fusion index (**p**), myotube area (**q**) and gene expression of myogenesis markers (**r**) from C2C12 *Cers2*^{KO} myoblasts. **s**–**x**, Total ceramide (**s**) and dihydroceramide (**t**) levels, immunocytochemistry (**u**), fusion index (**v**), myotube area (**w**) and gene expression of myogenesis markers (**x**) from C2C12 *Degs1*^{KO} myoblasts. Empty vector controls of the same wells have partly been used for different experiments. $n = 3$–6 per group. Student's two-tailed t-test with BH adjustment for FDR. All data are shown as mean ± s.e.m. *, BH FDR < 0.05; **, BH FDR < 0.01; and ***, BH FDR < 0.001. Scale bars, 50 µm. Cer, ceramides; dhCer, dihydroceramides; EV, empty vector; k, ×1,000.

($\beta = -0.27$, $P = 0.0002$) and left ($\beta = -0.19$, $P = 0.007$) hand grip strength (Fig. 7n). To study our findings in another sample, we examined individuals of the Helsinki Birth Cohort Study (HBCS; $n = 13{,}345$), a Finnish population cohort study featuring individuals born in the 1930s and 1940s, of whom 2,003 individuals underwent clinical age-related fitness measurements, including of grip strength. Similarly to the UKBB study, *SPTLC1* rs10820914 ($\beta = 1.65$, $P = 0.02$) and *DEGS1* rs35533869 ($\beta = -0.86$, $P = 0.04$) were associated with hand grip strength in older HBCS participants (Fig. 7n).

As hand grip strength may not always be reflective of overall strength[50], we studied the effect of *SPTLC1* rs10820914 and *DEGS1* rs35533869 on comprehensive measurements of age-related fitness, available in the well-characterized HBCS study in a subset of individuals between 70 and 80 years of age who underwent an extensive battery of physical fitness measurements (Table 1)[51]. The objectively measured fitness tests included arm curl, number of chair stands, chair sit and reach, back scratch and 6-min walk tests, collectively constituting the senior fitness test (SFT) score. The *SPTLC1* variant rs10820914, associated with hand grip strength in the UKBB and HBCS, was strongly associated with SFT score ($\beta = 4.14$, $P = 0.002$) and many of its component traits, including distance walked in 6 min ($\beta = 1.03$, $P = 0.01$), chair stand ($\beta = 0.55$, $P = 0.08$), arm curl ($\beta = 0.89$, $P = 0.01$) and chair sit and reach ($\beta = 1.31$, $P = 0.008$) (Fig. 7n). The *DEGS1* variant rs35533869 had a trend of associating with SFT score ($\beta = -3.14$, $P = 0.08$) and 6-min walking distance ($\beta = -0.96$, $P = 0.07$) and was associated with chair stand ($\beta = -0.98$, $P = 0.01$) (Fig. 7n).

In gene expression analysis using skeletal muscle data from the GTEx Project, rs10820914 was associated with *SPTLC1* expression in skeletal muscle, with the allele linked with improved phenotype associating with reduced *SPTLC1* expression ($\beta = -0.051$, $P = 0.026$) (Fig. 7n). A similar trend for rs10820914 on *SPTLC1* expression was observed in visceral adipose tissue ($\beta = -0.076$, $P = 0.01$). This suggests that the sphingolipid pathway possesses substantial pleiotropy, in line with the beneficial effects of pharmacological inhibition of sphingolipid de novo synthesis on inflammation in our aged mouse model (Fig. 2i) as well as with the reported pleiotropic effects of bioactive sphingolipid metabolites[14]. While rs10820914 was associated with the expression of the neighboring *ROR2* gene in some other tissues (for example, thyroid and adrenal glands), the global expression of *ROR2* is lower than that of *SPTLC1*, and the polymorphism was not associated with the expression of its neighboring genes in skeletal muscle (Supplementary Table 1). In *DEGS1*, the impaired age-related fitness-associated G allele of rs35533869 was associated with reduced skeletal muscle *DEGS1* expression ($\beta = -0.12$, $P = 0.006$), in line with our in vitro data. The SNP was also associated with *CAPN2* expression (500 kb from *DEGS1*; $\beta = 0.1$, $P = 0.009$) in skeletal muscle and poorly characterized *CNIH4*

https://doi.org/10.1038/s43587-022-00309-6

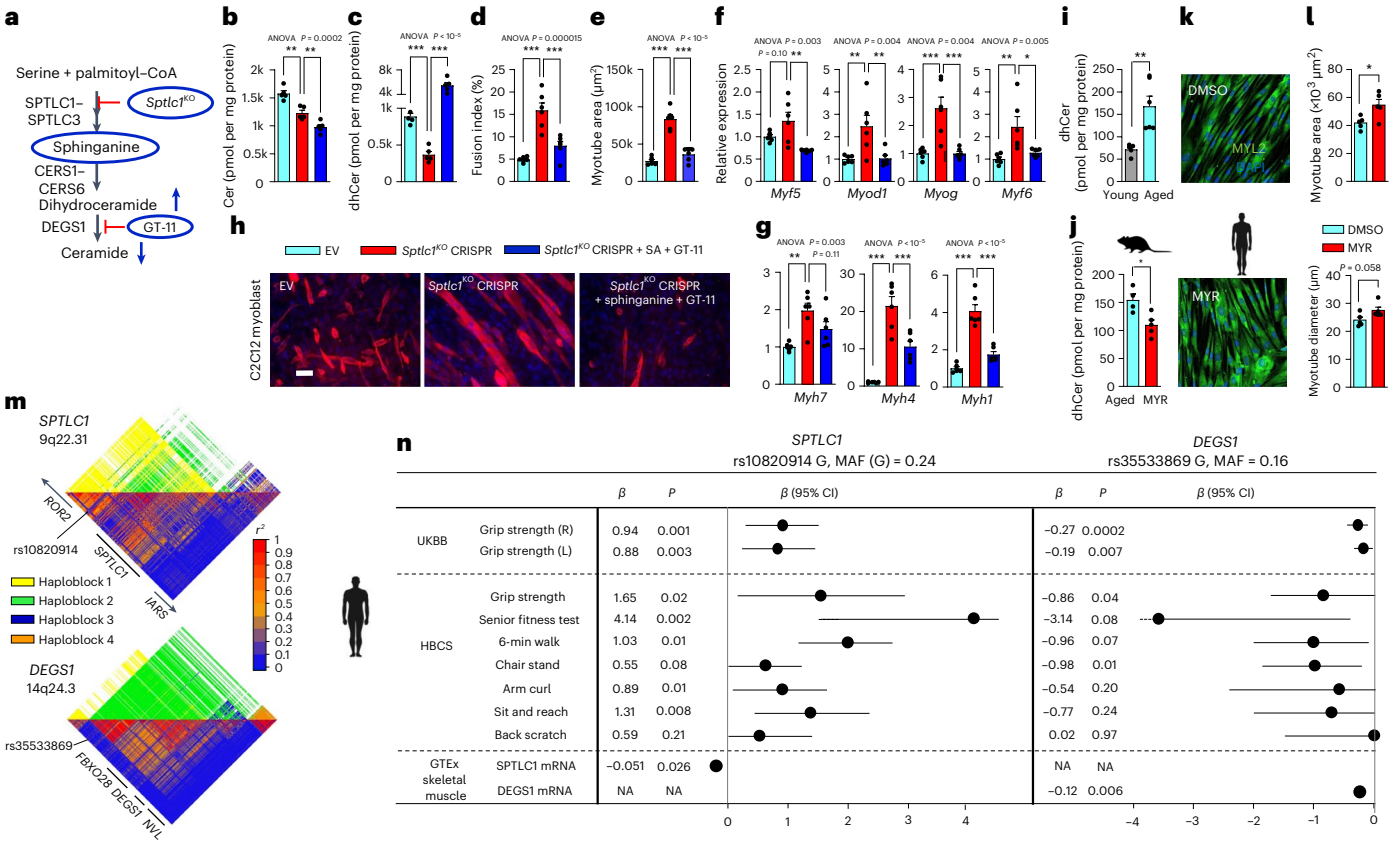

Fig. 7 | Dihydroceramide accumulation blunts the myogenic response to *Sptlc1* deficiency, and genetic variation in *SPTLC1* and *DEGS1* is associated with age-related fitness in humans. a, Experimental setup of sphinganine (4 μM) and GT-11 (1 μM) administration to C2C12 myoblasts to elevate cellular dihydroceramide levels. **b**–**h**, Ceramide (**b**) and dihydroceramide (**c**) levels, fusion index (**d**), myotube area (**e**), gene expression of myogenesis markers (**f**,**g**) and immunocytochemistry (**h**) in *Sptlc1*-deficient C2C12 myoblasts treated with sphinganine and GT-11. For each group, $n = 6$. For **b**–**g**, one-way ANOVA with Tukey's post hoc honestly significant difference was used. $^{*}P < 0.05$, $^{**}P < 0.01$ and $^{***}P < 0.001$. **i**, Skeletal muscle dihydroceramides of young (2-month-old) and aged (2-year-old) male mice; $n = 5$ or 6. **j**, Skeletal muscle dihydroceramides of aged (18 months) and aged mice treated with MYR (5 months at 0.4 mg kg^{-1} three times per week); $n = 4$ or 5. **k**,**l**, Immunocytochemistry (**k**) and myotube diameter and myotube area (**l**) of human primary myoblasts treated with DMSO or MYR (30 μM). For **k**,**l**, $n = 5 + 5$. Student's two-tailed t-test. All data are shown as mean ± s.e.m. $^{*}P < 0.05$, $^{**}P < 0.01$ and $^{***}P < 0.001$. Scale bars, 50 μm. **m**, Haploblock and linkage disequilibrium structure of *SPTLC1* and *DEGS1* in humans. **n**, Association of *SPTLC1* and *DEGS1* variants with grip strength in >65-year-old UKBB participants ($n = 95{,}211$) and senior fitness test (SFT) score and its component traits in the HBCS ($n = 400$) and skeletal muscle mRNA expression in the GTEx Project ($n = 706$). The forest plots represent β values and the error show the 95% confidence interval (CI). L, left; NA, not available; R, right; SA, sphinganine. Icon credits: mouse, clipart.com; human, FreeVectors.net.

expression in other tissues (lung and thyroid), but not with the skeletal muscle expression of *FBXO28* and *NVL*, the genes most proximal to *DEGS1* (Fig. 7m).

To assess whether *SPTLC1* rs10820914 and *DEGS1* rs35533869 are located in potentially regulatory regions, we explored the human registry for *cis*-regulatory elements provided by the ENCODE Project Consortium[52] and found that both these variants fall in regions of annotated *cis*-regulatory elements (Supplementary Fig. 10). While there was no enrichment of H3K27ac marks in these regions, both regions appear to be enriched in H3K4me1, a chromatin modification associated with the positional location of enhancer elements.

These genetic data, demonstrating that the *SPTLC1* rs10820914 variant is associated not only with grip strength but also with general age-related fitness in humans, imply that modulation of the sphingolipid de novo synthesis pathway in human aging could deliver considerable fitness benefits. Furthermore, consistent with our in vitro studies, these findings suggest that DEGS1, the enzyme catalyzing the conversion of dihydroceramides to ceramides, has a role opposite to that of SPT in age-related fitness. Thus, increased *DEGS1* expression in muscle is associated with improved muscle function in older adults.

Discussion

In this study, we establish the relationship between sphingolipid metabolism and age-related loss in muscle mass and function. Sphingolipids have been associated with metabolic disease, cancer and cardiovascular disease[14]. Diabetes is reported to be a risk factor for sarcopenia[53], and sphingolipids could partly contribute to the onset of sarcopenia through exacerbation of metabolic disease and other pleiotropic effects. Our approach of starting interventions inhibiting sphingolipid synthesis later in life allows us to specifically assess the effects of sphingolipid synthesis inhibition during aging, which is not possible in many genetically modified mouse models, in which the genetic modification is already present during development, given the importance of sphingolipids during development[54]. Our finding of increased sphingolipid levels in 24-month-old mice, an age at which age-related muscle dysfunction is already present[55], suggests that skeletal muscle sphingolipid levels are linked with the severity of sarcopenia; previous studies did not observe increased levels of ceramides in 18-month-old mice[28], as they used mice at an age at which age-related muscle dysfunction is not yet observed[55]. Our findings are in line with the reduction of saturated ceramides by high-intensity training observed in aged human subjects displaying elevated ceramide

https://doi.org/10.1038/s43587-022-00309-6

Table 1 | Clinical characteristics of the HBCS (*n* = 2,003)

Characteristic	Mean or %	s.d.
n	2,003	
Women (%)	59	
Age (years)	71	2.7
Body mass index (kg per m^2)	27	4.5
Waist–hip ratio	0.96	0.08
Systolic blood pressure (mmHg)	156	22
Diastolic blood pressure (mmHg)	85	10.8
Total cholesterol (mmol l^{-1})	5.42	1.02
Diabetes (%)	15	
SFT	45.4	17.3
6-min walk (m)	572	105
Back scratch (cm)	−3.56	4.85
Chair stand (*n*)	11.4	2.22
Sit and reach (cm)	−0.44	4.89
Arm curl (*n*)	15.7	3.52
Grip strength (N)	303	117

levels[56] and establish the benefits of inhibiting the sphingolipid pathway for age-related fitness. As C18 ceramides are the most abundant ceramides in muscle tissue, and C16 ceramides are the most abundant in C2C12 myoblasts, our work points to very-long-chain sphingolipids (C24) potentially having an inhibitory role in myogenic differentiation. This is supported by inactivation of *Cers2* promoting myogenesis and resulting in reduced cellular C24 sphingolipid content in the presence of elevated C16 sphingolipids, as well as the accumulation of very-long-chain sphingolipids in skeletal muscle upon aging.

Genetic and pharmacological inactivation of SPT slowed the age-related muscle dysfunction in aged mice. Myriocin reduced the presence of inflammatory cells in muscle and enhanced the myogenic potential of myoblasts. Inflammation has been shown to negatively affect protein synthesis[57] and at least partially be involved in age-related muscle wasting[58]. Furthermore, inflammation has deleterious effects on MuSCs. On the other hand, inhibition of sphingolipid synthesis promoted muscle differentiation, protein synthesis and age-related fitness in a tissue-specific manner (Fig. 4). As it has been shown that electrical stimulation of muscle attenuates the muscle-wasting proinflammatory stimuli, such as interferon γ (IFNγ)[59], the cell-autonomous improvement in muscle function from inactivation of sphingolipid synthesis could have secondary anti-inflammatory effects.

While systemic treatment with myriocin affects the whole body, we provide evidence through ex vivo studies that inhibition of sphingolipid de novo synthesis has an independent effect on myogenic differentiation. This is validated by MYR-induced differentiation of myoblasts as well as of freshly isolated MuSCs. The specificity of these effects to the sphingolipid de novo synthesis pathway, and not to off-target effects of MYR, is verified by the myogenesis-promoting effects of genetic inactivation of two key enzymes of the pathway, *Sptlc1* and *Cers2*, in C2C12 differentiation assays. Furthermore, the improvement of age-related fitness upon AAV-mediated silencing of *Sptlc1* in the gastrocnemius shows that inactivation of sphingolipid synthesis provides muscle-specific benefits in vivo. These beneficial effects are supported by genetic analysis in the UKBB and HBCS, in which we demonstrate the association of *SPTLC1* variants with age-related fitness and reduced expression, extending our findings from mice to humans.

Our work also provides strong support for the physiological role of DEGS1 in skeletal muscle[44]. While the myogenic program in myoblasts was activated by both pharmacological and genetic inhibition of *Sptlc1*, this effect was lost by inactivation of DEGS1, the enzyme converting dihydroceramides to ceramides by double bond insertion. While addition of sphinganine and the DEGS1 inhibitor GT-11 to myoblasts reduced ceramide levels even more than the genetic knockout of *Sptlc1* alone (Fig. 7a–h), these myoblasts lost their myogenic potential in the presence of high dihydroceramide levels. This was manifested by the blunted expression of myogenic transcription factors and markers of mature myotubes in dihydroceramide-loaded myoblasts. Although dihydroceramides are far less abundant than ceramides, their bioactive role in cellular physiology has recently begun to emerge[44,45], and given that their levels were elevated in skeletal muscle upon aging, they could be important mediators of the effects of increased sphingolipid de novo synthesis in age-related sarcopenia. These findings are supported by genetic data from humans demonstrating that the *DEGS1* variant associated with reduced expression is also associated with poorer fitness upon aging.

Our findings suggest that inhibition of SPT and sphingolipid synthesis could be a therapeutic strategy to treat age-related muscle dysfunction and sarcopenia. As muscle dysfunction is associated with chronic comorbidities, patients with sarcopenia are often managed with a number of medications[60]. Although use of multiple drugs may be necessary to obtain satisfactory treatment outcomes for chronic disease, it simultaneously predisposes patients to adverse drug reactions, interactions and prescription cascades[60]. One way to reduce age-associated polypharmacy, while providing effective treatment to chronic diseases, could be the development of multitargeted therapeutics, that is, single pharmaceutical agents targeting multiple diseases[61]. Given the involvement of sphingolipids in a number of diseases[14,15], targeting sphingolipid metabolism could produce benefits far beyond age-related muscle dysfunction, having the potential to moderate multiple-drug prescriptions. Our study presents a strong case to embark on the development of potent inhibitors of sphingolipid synthesis for age-related muscle dysfunction and co-occurring pathologies.

Methods

In vivo studies

Animals. Young (2-month-old) and aged (18-month-old or 24-month-old, all killed at 24 months) male C57BL/6JRj mice were purchased from Janvier Labs. EchoMRI was used to measure fat and lean body mass, which was performed before and after the treatment. The dose of myriocin was 0.4 mg kg^{-1} three times a week. Myriocin (Enzo Life Sciences) was first dissolved in DMSO and was then mixed with phosphate-buffered saline (PBS) so that each mouse received 1.5 µl of DMSO per injection. Animals were fed a standard chow diet (Safe 150) with the following composition: 56.9% nitrogen-free extract, of which 41.0% was starch and 3.4% was sugars, 18.0% crude protein, 4.8% crude fat, 4.2% crude ash, 4.1% crude fiber and 12.0% moisture. AAV9 injections were performed on animals randomized according to their body weights. C57BL/6j (18-month-old) male mice were bilaterally muscle injected with 2×10^{11} viral particles (Vector Biolabs) containing scrambled shRNA or *Sptlc1*-targeting shRNA in gastrocnemius muscle. Four to five months after the injections, phenotypic tests were performed on the animals. When mice were killed, muscles were removed for histochemical analyses or snap frozen in liquid nitrogen for biochemical assays. All animals were housed in micro-isolator cages in a room illuminated from 7:00 a.m. to 7:00 p.m. with ad libitum access to food and water. All the animal experiments are authorized by animal license 2890.1 and 3341 in the Canton of Vaud, Switzerland. Mice displaying signs of severe illness were removed from the experiments.

Measurement of sphingolipids in vivo. Plasma (100 µl) and weighed tissue samples (20–60 mg) were transferred to 2-ml Safe-Lock PP-tubes and extracted as previously described[62]. Briefly, samples were homogenized using two aliquots of 6-mm steel beads on a Mixer Mill (Retsch; 2 ×10 s, vibrational frequency of 30 1/s) in 700 µl methanol (3/1, vol/vol)

containing 1% acetic acid, 500 pmol butylated hydroxytoluene and 200 pmol of internal standards (IS, d18:1/17:0 ceramide, d18:1/17:0 sphingomyelin, Avanti Polar Lipids) per sample. Total lipid extraction was performed for 30 min at room temperature under continuous shaking. After adding 140 µl of dH_2O and further incubating for 30 min at room temperature, samples were centrifuged for 15 min at 1,000 x g to create phase separation. Then, 500 µl of the organic upper phase was collected and dried under a nitrogen stream. For ultra-performance liquid chromatography (UPLC)–mass spectrometry analysis, lipids were resolved in 700 µl of 2-propanol–methanol–water (7:2.5:1, vol/vol/vol). Remaining tissues were dried and solubilized in NaOH (0.3 N) at 65 °C for 4 h, and the protein content was determined using Pierce BCA reagent (Thermo Fisher Scientific) and bovine serum albumin (BSA) as the standard.

Chromatographic separation was adapted from Knittelfelder et al.[63] using the ACQUITY–UPLC system (Waters Corporation), equipped with a Luna Omega C18 column (2.1 × 50 mm, 1.6 µm; Phenomenex) setting off a 20-min linear gradient with 80% solvent A (methoanol:H_2O (1:1, vol/vol), 10 mM ammonium acetate, 0.1% formic acid, 8 µM phosphoric acid). The column compartment was maintained at a temperature of 50 °C. An EVOQ Elite triple-quadrupole mass spectrometer (Bruker) equipped with an electrospray ionization (ESI) source was used to detect lipids in positive ionization mode. Lipid species in question were analyzed by selected reaction monitoring (SRM) (ceramide, $[M + H]^+$ to *m/z* 264.3, 22 eV, 60 ms; sphingomyelin, $[M + H]^+$ to *m/z* 184.1, 20 eV, 40 ms; resolution 0.7 Q1/Q3). Data acquisition was conducted by MS Workstation (Bruker). Data were normalized for extraction, recovery and ionization efficacy by computing analyte/IS ratios and expressed as pmol per mg protein in tissues and pmol per ml in plasma.

Measurement of deoxysphingolipids. Plasma and muscle sphingolipids were processed using a method adapted from ref. [64]. Briefly, 10–15 mg of muscle sample was extracted with 500 µl of −20 °C methanol, 400 µl of ice-cold saline and 100 µl of ice-cold water and spiked with IS doxSA d3 (Avanti Polar Lipids). An aliquot (50 µl) of homogenate was dried under air and resuspended in RIPA buffer for protein quantification using the BCA assay (BCA Protein Assay, Lambda Biotech). To the remaining homogenate, 1 ml of chloroform was added, and the samples were vortexed for 5 min followed by centrifugation at 4 °C for 5 min at 15,000*g*. The organic phase was collected and 2 µl of formic acid was added to the remaining polar phase, which was re-extracted with 1 ml of chloroform. Combined organic phases were dried, and the pellet was resuspended in 500 µl of methanol, and subsequent extraction steps were identical to those described for plasma.

Fifty microliters of plasma was mixed with 500 µl of methanol and spiked with IS of doxSA d3 (Avanti Polar Lipids). The samples were placed on a mixer for 1 h at 37 °C and centrifuged at 2,800*g*, and the supernatant was collected and hydrolyzed with acid overnight at 65 °C using 75 µl of methanolic HCl (1 N HCl,10 M H_2O in methanol). Next, to neutralize reactions, 100 µl of 10 M KOH was added. Then, 625 µl of chloroform, 100 µl of 2 N NH_4OH and 500 µl of alkaline water were added, and the sample was mixed with vortexing and centrifuged for 5 min at 16,000*g*. The lower organic phase was washed three times with alkaline H_2O and dried under air. An Agilent 6460 triple-quadrupole (QqQ) liquid chromatography (LC)–tandem mass spectrometer (MS/MS) was used to perform LC–mass spectrometry analysis. A C18 column (Luna 100 × 2.1 mm, 3µm, Phenomenex) was used to achieve metabolite separation. Mobile phase A consisted of a 60:40 ratio of methanol to water, and mobile phase B was composed of 100% methanol with 0.1% formic acid with 5 mM ammonium formate added to both mobile A and B. The program for gradient elution consisted of holding at 40% B for 0.5 min, linearly increasing to 100% B over 15 min and keeping this for 9 min, followed by re-equilibration for 10 min to the original condition. The capillary voltage was 3.5 kV, the drying gas temperature was set to 350 °C, a drying gas flow rate of 10 L min^{-1} was used and the nebulizer pressure was set to 60 psi. Sphingoid bases were analyzed by SRM of the transition from precursor to product ions at associated optimized collision energies and fragmentor voltages (see following table). Sphingoid bases were then quantified from spiked IS of known concentration.

Sphingoid base	Precursor ion	Product ion	*n*
m17:0 doxSA	272.4	254.4	13
m18:0 doxSA	286.3	268.4	13
m18:0 doxSA d3	289.3	271.5	13

Measurements of sphingolipids in vitro. Cell pellets (1.2×10^6 cells) were lysed by the addition of 100 µl and 200 µl methanol (100 %), spiked with the stable isotope-labeled IS (Spa(d17:0), Cer(d18:1/16:0)-d9, Cer(d18:1/18:0)-d7, Cer(d18:1/24:0)-d7 and Cer(d18:1/24:1)-d7). Sample homogenization was performed in the Cryolys Precellys Tissue Homogenizer (2 × 20 s at 10,000 r.p.m., Bertin Technologies) with ceramic beads. The bead beater was air-cooled at a flow rate of 110 L min^{-1} at 6 bar. Homogenized extracts were centrifuged for 15 min at 4,000*g* at 4 °C, and the resulting supernatants were collected for the LC–MS/MS analysis. LC–MS/MS was used to quantify sphingolipids in positive ionization mode with a 6495 triple-quadrupole system interfaced with a 1290 ultra-high performance liquid chromatography (UHPLC) system (Agilent Technologies), adapted as previously described[65]. In brief, the chromatographic separation was performed in a ZORBAX Eclipse Plus C8 column (Agilent) (1.8 µm, 100 mm × 2.1 mm inner diameter). Mobile phase A consisted of 5 mM ammonium formate and 0.2% formic acid in H_2O while mobile B consisted of 5 mM ammonium formate and 0.2% formic acid in methanol, and a flow rate of 400 µl min^{-1} was used. The injection volume of the sample was 2 µl, and the column temperature was 40 °C. A linear gradient was applied and held until minute 14, with elution starting from 80% to 100% of B in 8 min. The column was then equilibrated to initial conditions. ESI source conditions were used as follows: dry gas temperature, 230 °C; nebulizer, 35 psi and flow rate of 14 L min^{-1}; sheath gas temperature, 400 °C and flow rate of 12 L min^{-1}; nozzle voltage, 500 V; and capillary voltage, 4,000 V. Dynamic multiple-reaction monitoring was used as the acquisition mode with a total cycle time of 500 ms. Optimized collision energies for each metabolite were used. Raw LC–MS/MS data were processed applying Agilent Quantitative Analysis software (version B.07.00, MassHunter Agilent Technologies). For absolute quantification, calibration curves and the stable isotope-labeled IS were used to determine the response factor. For each metabolite, linearity of the standard curves was evaluated using a 12-point range. In addition, peak area integration was manually curated and corrected when needed. Sphingolipid concentrations were reported, and protein concentrations were measured in protein pellets (with BCA, Thermo Fisher Scientific) following the metabolite extraction. Theoretical transitions for 15 dihydrosphingomyelin species were added using the in silico MS/MS LipidBlast database, and retention times were predicted based on similarities with other sphingolipid species targeted with the same analytical method. Semiquantification was done on integrated SRM peak areas.

Endurance running test. The exercise regimen on a treadmill commenced at a speed of 15 cm s^{-1}. After every 12 min, the speed was increased by 3 cm s^{-1}. As the mice increased in age, we used an incline of 0 degrees. Mice were considered to be exhausted and removed from the treadmill if they received seven or more shocks (0.2 mA) per minute for two consecutive minutes. The distance traveled and time before exhaustion were registered as maximal running distance and time[41,66].

Grip strength. Muscle strength was assessed by grip strength test. The grip strength of each mouse was measured on a pulldown grid assembly

connected to a grip strength meter (Columbus Instruments). The mouse was drawn along a straight line parallel to the grip, providing peak force. The experiment was repeated three times, and the highest value was included in the analysis.

Rotarod test. The rotarod test measures muscle strength, coordination and endurance[67]. Mice were left undisturbed in the room for 30 min. The speed of the rotating cylinder (rotarod) increased from 0 to 40 r.p.m. in 5 min. Each mouse had three trials per day for three consecutive days. The latency and speed with which the mouse reached its passive rotation or fell from the rotor were recorded, and the latency and speed of the best trial of the second day are presented.

Crossbar test. The crossbar test assesses active balance through the ability to balance while walking along an elevated beam to reach a dark end side where mice are able to hide[68]. Because all the mice were easily able to cross a square (3 cm) beam and a circular beam of 1.5 cm diameter was too difficult for them, we recorded the latency to cross a circular beam of 3 cm. The mice were trained for 1 d before the actual trial was recorded, and the average of the latency of three trials per mouse is presented.

Ex vivo muscle force assessment. Muscle mechanical measurements were performed as previously described[69,70] with slight modifications. All assays were performed in a blinded fashion. Control C57 BL/10j aged mice and myriocin-treated aged mice (24 months old) were killed by cervical dislocation. EDL muscles were quickly dissected and then bathed in a 10-ml horizontal chamber containing a continuously oxygenated Krebs solution composed of 135.5 mM NaCl, 5.9 mM KCl, 1 mM $MgCl_2$, 2.5 mM $CaCl_2$, 11.6 mM HEPES sodium and 11.5 mM glucose, with pH of 7.4, at 25 °C. The muscle was tied between a dual-mode lever arm and a fixed hook, and a stimulation was delivered through platinum electrodes running parallel to the muscle (1500 A Intact Muscle Test System, Aurora Scientific). Resting muscle length (L_0) was carefully adjusted for maximal isometric force with 125-Hz maximally fused tetani. The force–frequency relationship was determined by sequentially stimulating the muscles in 25-, 50-, 75-, 100-, 125- and 150-Hz stimulation trains of 300 ms in duration with 1 min of rest between each contractions. Normalized muscle-specific force (mN/mm^2) was expressed relative to the CSA, obtained by dividing muscle blotted weight (mg) by muscle length and considering the fiber length equal to $0.5L_0$ for EDL and 1 for soleus muscles[71]. To investigate muscle fatigue, muscles were subjected to 125-Hz stimulation trains of 300 ms in duration at 10-s intervals over 50 tetani for EDL muscles and at a 1-s interval over 120 tetani for soleus muscles. Data from each experiment were analyzed with Aurora's DMA software (Aurora Scientific, 2002; Solwood Enterprises, 2002) and Microsoft Excel.

Stem cell isolation. Gastrocnemius, soleus and quadriceps muscles from both hindlimbs were excised and transferred into PBS on ice. All muscles were trimmed, minced and digested with 2.5 U ml^{-1} of Dispase II (Roche) and 0.2% collagenase B (Roche) in PBS for 30 min at 37 °C. Samples were then centrifuged at 50*g* for 5 min followed by removing the supernatant and further digested for 20 min at 37 °C twice. Muscle slurries were sequentially filtered through 100-µm and 40-µm cell strainers. The isolated cells were then washed in washing buffer (PBS + 2.5% BSA) and resuspended in 800 µl of washing buffer. They were immediately stained with antibodies, including antibodies to CD31 (1:800, eBioscience, eFluor450 conjugated), CD45 (1:200, eBioscience, eFluor450 conjugated), Sca-1 (1:1,000, eBioscience, PE-Cy7 conjugated), CD11b (1:100, eBioscience, eFluor450 conjugated), and CD34 (1:100, BD Pharmingen, FITC conjugated), and α7 integrin (1:50, R&D Systems, eFluor700 conjugated) for 45 min at 4 °C. Secondary staining was performed with propidium iodide (PI, Sigma) for 15 min at 4 °C in the dark. Stained cells were analyzed and sorted using the FACSAria II instrument (BD Biosciences). Debris and dead cells were excluded by forward scatter, side scatter and PI gating.

Histology. TA muscles were dissected from anesthetized mice, and immediately embedded in Thermo Scientific Shandon Cryomatrix and frozen in isopentane, cooled in liquid nitrogen, for 1 min before being transferred to dry ice and stored at −80 °C. Eight-micrometer cryosections were incubated in 4% paraformaldehyde (PFA) for 15 min; washed three times for 10 min with PBS; counterstained with 4′,6-diamidino-2-phenylindole (DAPI) and antibodies to laminin (1:200, Sigma), dystrophin (1:100, Spring Bioscience), CD45 (1:200, Life Technologies), F4/80 (1:100, Bio-Rad ABD Serotec) or eMyHC (1:50, Developmental Studies Hybridoma Bank, University of Iowa), coupled with Alexa-488 or Alexa-568 fluorochrome (Life Technology); and mounted with Dako Mounting Medium. Succinate dehydrogenase (SDH) staining was used to determine muscle fiber composition. For each sample, four randomly selected fields were quantified. ImageJ software was used to analyze fluorescence microscopy images from muscle fibers, and minimal Feret diameter, and the CSA in TA muscles were measured using software quantification of images of muscle stained for dystrophin, laminin and DAPI from the Olympus VS120-S6-W slide scanner. For each measurement and condition, 2,000 fibers were used at minimum. The minimal Feret diameter is expressed as the minimum distance between two parallel tangents at opposing borders of the muscle fiber. This measure has been found to be relatively unaffected by deviations away from the optimal cross-sectioning profile during the sectioning process. Seven to eight mouse samples per condition were used for histological quantification of donor mice. The eMyHC quantification is expressed as the proportion of eMyHC-positive signal over the total TA CSA.

Western blotting. Mouse gastrocnemius muscles were lysed on ice in RIPA buffer composed of 50 mM Tris HCl, 5 M NaCl, 5 mM EDTA, 0.1% SFS, 100 mM NAF, 5 mg ml^{-1} sodium deoxycholate and 1% NP40 containing protease and phosphatase inhibitors (Roche). Homogenization was performed at 300*g* for 1 min. Protein concentrations were determined using the Bradford method, and samples were loaded on a 12% SDS-PAGE gel. After electrophoresis, proteins were transferred onto methanol-activated polyvinylidene difluoride membranes. Blocking of the membranes was done in 5% milk in Tris-buffered saline Tween-20 (TBST) for 1 h, and after washing, the membranes were incubated overnight with primary antibody to SPTLC1 (Proteintech), SPTLC2 (Thermo Fisher Scientific, diluted1:1,000 5% BSA–TBST) or anti-CERS2 (Sigma, diluted 1:1,000 in 3% BSA–TBST). Incubation with secondary anti-rabbit polyclonal antibody was done in 5% BSA–TBST at a 1:2,000 dilution. Antibody detection reactions were developed by enhanced chemiluminescence (Advansta) and imaged using the c300 imaging system (Azure Biosystems).

Ex vivo analysis of MuSCs. MuSCs were isolated as described above and seeded in 96- or 48-well plates. The cells were incubated in 30 µM myriocin-containing medium (Ham's F-10 Nutrient Mixture, 20% FBS, 2.5 ng ml^{-1} basic fibroblast growth factor, 100 U/ml^{-1} penicillin, 100 µg ml^{-1} streptomycin) for 72 h. Then, 4% PFA was applied for 15 min, and the cells were washed three times for 10 min with PBS and were blocked in 2% BSA in PBS. The cells were then incubated in primary antibody to MYOG (1:50, Santa Cruz) overnight at 4 °C. Secondary antibodies were coupled with Alexa-488 or Alexa-568 fluorochrome (Life Technology) and cell were mounted with Dako Mounting Medium. A Leica DMI 4000 microscope was used to image the cells. Quantification of the $MYOG^+$ cell number was based on more than 500 cells per condition.

Gene expression and phenotype analysis in the BXD mouse population. Quadriceps microarray data (Affymetrix Mouse Gene 1.0 ST) and phenotype data from a BXD mouse genetic reference population[36] were

analyzed for Pearson correlations with R software. The first principal component of the ceramide biosynthetic pathway representing its expression in muscle was calculated by including the following genes: *Sptlc1*, *Sptlc2*, *Kdsr*, *Cers1*, *Cers2*, *Cers3*, *Cers4*, *Cers5*, *Cers6* and *Degs1*. For correlation between skeletal muscle gene expression of myogenic transcription factors, a fitness score was calculated as the sum of *Z*-scores for gastrocnemius mass (phenotype ID, 20088) and running distance (phenotype ID, 17738) in the BXD population.

Quadriceps transcript profiling using RNA sequencing. Quadriceps muscles were collected and snap-frozen in liquid nitrogen from C57BL/6JRj mice undergoing intraperitoneal myriocin treatment for 10 weeks on a chow diet starting at the age of 18 months. RNA was isolated using the Direct-zol RNA Kit (Zymo). RNA quality was assessed using the Agilent 2100 BioAnalyzer (Agilent). Samples with an RNA integrity number ≥ 8, a 28 S/18S ratio ≥ 1.0 and concentration ≥ 20 ng μl^{-1} were included in the analyses. Using these criteria, nine (four DMSO and five MYR) samples passed and two samples failed to pass quality control (QC) criteria. Sequencing libraries were prepared by BGI Genomics using the DNBseq technology. Paired-end sequencing with 100 cycles was performed using the BGISEQ-500 instrument. After the removal of adaptor sequences and low-quality reads, we obtained at least 56 million reads per sample. SOAPnuke was used to obtain clean reads (parameters -l15, -q 0.2, -n 0.05). Reads were mapped using STAR aligner version 2.5.2b using the mouse GRCm38 genome assembly and release 91 GTF annotation from Ensembl. HTSeq-count version 0.6.0 was used to count the number of reads mapping to genes (mode=union, Type=exon, idattr=gene_id). Transcripts displaying higher expression than $\log_2(CPM + 1) > 0.5$ in at least three samples were included in the analyses. Differential gene expression analysis and expression normalization were performed using voom, 'variance modeling at the observational level' (ref. [72]), adjusting for the date on which the mouse was killed. At the individual gene level, no gene passed the multiple-testing correction threshold. The BH correction for multiple testing was used. For GSEA using GO categories, transcripts were ordered according to their $\log_2$-transformed fold change, and 100,000 permutations were used. Adjusted *P* value < 0.05 was considered significant.

Analysis of tissue MYR content. Muscle tissue was extracted by the addition of 100 µl methanol for every 10 mg of tissue (fresh weight). Sample homogenization was performed in the Cryolys Precellys Tissue Homogenizer (2 × 20 s at 10,000 r.p.m., Bertin Technologies) with ceramic beads. The bead beater was air-cooled at a flow rate of 110 L min^{-1} at 6 bar. Homogenized extracts were centrifuged for 15 min at 4,000*g* at 10 °C, and the resulting supernatants were evaporated to dryness in a CentriVap Vacuum Concentrator (Labconco). The dried extracts were reconstituted in 40 µl methanol (100%), sonicated (for 1 min) and centrifuged for 15 min at 4,000*g* at 10 °C, and the resulting supernatants were transferred to vials for the LC–MS/MS analysis.

Extracted samples were analyzed using reversed-phase LC coupled with MS/MS[73] in negative ionization mode using a TSQ Altis triple-quadrupole system interfaced with a Vanquish Duo UHPLC System (Thermo Fisher Scientific). Chromatographic separation was carried out in an Acquity BEH C18 column (1.7 µm, 150 mm × 2.1 mm inner diameter; Waters). Mobile phase A was composed of water with 0.1% acetic acid while mobile phase B was composed of acetonitrile:isopropanol (90:10 vol/vol) at a flow rate of 500 µl min^{-1}, a column temperature of 60 °C and a sample injection volume of 2 µl. Gradient elution was performed with 80% A as the starting condition, linearly decreased to 65% at 2.5 min, to 60% at 4.5 min, to 58% at 6 min, to 50% at 8 min, to 35% at 14 min, to 27.5% at 15.5 min and to 0% at 16.6 min. The column was then washed with solvent B for 0.9 min and equilibrated to initial conditions. Optimized HESI source parameters were set as follows: voltage, −3,000 V in negative mode; sheath gas (arbitrary units), 50; auxiliary gas (arbitrary units), 10; sweep gas (arbitrary units), 1; and an ion transfer tube temperature, 325 °C. Nitrogen was used as the nebulizer and argon was used as the collision gas (1.5 mTor). The vaporizer temperature was 350 °C. Detection was accomplished by multiple-reaction monitoring (MRM), using the following transitions: *m/z* 400 to 104 and *m/z* 402 to 104 for myriocin and 14-OH-MYR, respectively[74]. Raw LC–MS/MS data were processed using XCalibur software (Thermo Fisher Scientific). Peak areas (in arbitrary units) of corresponding transitions were used for comparative analysis.

Statistics and reproducibility. Comparisons were done between wild-type and aged mice and between aged mice and aged treated with myriocin with Student's two-tailed *t*-tests on the raw data, and the BH FDR was controlled for in each figure panel. For qPCR results, *P* values were calculated using Student's two-tailed *t*-test with log-transformed expression values with BH FDR adjustment. In all the analyses, adjusted *P* values <0.05 were considered significant. During phenotyping, the experimenters were performed with blinding except during endurance training on a treadmill. The allocation of mice to treatment groups was based on their body weight so that average body weights at the beginning of the experiments were equal. Mice displaying signs of severe illness were removed from the experiments. No statistical methods were used to predetermine sample sizes, but our sample sizes are similar to those reported in previous publications[19,41]. Data distribution was assumed to be normal, but this was not formally tested.

In vitro studies

Cell culture and cell transfection. The C2C12 mouse myoblast cell line was obtained from the American Type Culture Collection (CRL-1772TM). C2C12 cells or clones were cultured in growth medium consisting of DMEM (Gibco, 41966-029), 20% FBS (Gibco, 10270-106), 100 U ml^{-1} penicillin and 100 mg ml^{-1} streptomycin (Gibco, 15140-122). To induce differentiation, FBS was substituted with 2% horse serum (Gibco, 16050-122). Trypsin–EDTA (0.05%, Gibco, 25300-062) was used to detach cells. Human skeletal muscle cells were obtained from Lonza (SkMC, CC-2561) and cultured in growth medium consisting of DMEM/F12 (Gibco, 10565018), 20% FBS (Gibco, 10270-106) and 100 U ml^{-1} penicillin and 100 mg ml^{-1} streptomycin (Gibco, 15140-122). To induce differentiation, FBS was reduced to 2% and kept in culture. All cells were maintained at 37 °C with 5% CO_2. Cell transfections were done using the TransIT-X2 system (Mirus) according to the manufacturer's protocol with a 3:1 ratio of transfection agent to DNA. C2C12 cells were grown until confluent, myriocin or DMSO was added, and cells were kept in the growth medium for another 3 d. *Sptlc1* clones were plated to reach confluency simultaneously and were kept in growth medium for 3 d before using them for immunocytochemistry or RNA isolation. The concentration of myriocin in the medium for all experiments was 100 nM except for Fig. 5, in which a concentration of 30 µM was used. The SPT inhibitor Takeda 2 has been previously described[42,43] and was used at a concentration of 100 nM. Nontargeting or *Sgms1*-targeting (208449) and *Sgms2*-targeting (74442) ON-TARGETplus SMARTpool (Horizon Discovery Biosciences) siRNA was used at a final concentration of 50 nM. A stock solution of 20 mM myriocin in DMSO was used to dissolve myriocin, and a corresponding volume of DMSO without myriocin was used as a control. Cell lines were tested for mycoplasma contamination. No contamination was observed.

CRISPR guide RNA design and cloning. Two guide RNAs per gene were designed with the help of the online GPP web portal tool (https://portals.broadinstitute.org/gpp/public/analysis-tools/sgrna-design) using the *Streptococcus pyogenes* protospacer-adjacent motif sequence (NGG). The guide RNAs with the best predicted on- and off-target scores were selected. The guide RNA sequences are listed in Supplementary Table 3. The oligonucleotides were synthesized (Microsynth) and cloned into the CRISPRv2 plasmid (Addgene, 52961) using the BsmBI restriction sites[75]. Insertion by cloning was verified by the Sanger

sequencing (Microsynth). To test the efficiency of the guide RNAs, the cloned vectors were transiently transfected (TransIT, Mirus) in C2C12 cells, and 48 h after transfection, RNA was isolated and reverse transcribed, and gene expression was measured using western blot analysis.

Creation of monoclonal *Sptlc1*^{KO} C2C12 myoblasts. C2C12 cells were transfected with the lentiCRISPRv2 plasmid containing guide RNAs targeting exon 1 of *Sptlc1* or the empty vector lentiCRISPRv2 plasmid as a control. Cells were selected 36 h after transfection with 2 μg ml^{-1} of puromycin (Invivogen; QLL3803A) for 3 d and single-cell sorted. Five to ten different clones for each guide RNA were grown without a selection marker. DNA from these clones was isolated (Macherey–Nagel, 740952) and PCR amplified (Supplementary Table 2). The PCR product was gel purified (Macherey–Nagel, 740609), and Sanger sequencing was performed to verify the clones with deletions or insertions. In one of the clones, *Sptlc1* gRNA1 led to homozygous knockout of *Sptlc1* (*Sptlc1*$^{-/-}$), whereas gRNA2 led to heterozygous knockout of *Sptlc1* (*Sptlc1*$^{+/-}$) in another clone.

Creation of polyclonal *Sptlc1*^{KO} and *Cers2*^{KO} C2C12 myoblasts. Lentivirus particles were produced from lentiCRISPRv2 plasmids containing no guide RNA (empty vector), *Sptlc1* gRNA2 or *Cers2* gRNA2 (Supplementary Table 4) by co-transfection with the packaging plasmids pMD2G and psPAX2 in HEK 293 T cells using Lipofectamine 2000. Viral supernatants were collected 36 to 48 h after transfection. C2C12 cells were transduced with viral supernatant for 20 h. Cells were selected 24 h later with 3 μg ml^{-1} of puromycin for three days. The same electric vehicle control was used for the knockout clones. Reduction in the target protein was confirmed by western blotting.

Western blotting. C2C12 cells were lysed on ice in RIPA buffer composed of 50 mM Tris HCl, 5 M NaCl, 5 mM EDTA, 0.1% SFS, 100 mM NAF, 5 mg ml^{-1} sodium deoxycholate and 1% NP40 containing protease and phosphatase inhibitors (Roche). Protein concentrations were determined using the Bradford method, and samples were loaded on a 12% SDS–PAGE gel. After electrophoresis, proteins were transferred onto methanol-activated polyvinylidene difluoride membranes. Blocking of the membranes was done in 5% milk in TBST for 1 h, and after washing, the membranes were incubated overnight with primary antibody against SPTLC1 (Proteintech) diluted 1:1,000 in 5% BSA–TBST 1:1000 or CERS2 (Sigma) diluted 1:1,000 in 3% BSA–TBST. Incubation with secondary anti-rabbit polyclonal antibody was done in 5% BSA–TBST at a 1:2000 dilution. The membrane was stripped before incubation with anti-vinculin antibody as the loading control. Antibody detection reactions were developed by enhanced chemiluminescence (Advansta) and imaged using the c300 imaging system (Azure Biosystems).

Protein synthesis assay. Protein synthesis was assessed using the SunSET assay as previously described (https://doi.org/10.1038/nmeth.1314). C2C12 cells were seeded on six-well plates and treated with myriocin for 72 and 96 h. After myriocin treatment, the medium was removed, and the cells were washed with 1× PBS. The cells were then incubated in medium containing 1 μM puromycin for 30 min under normal culture conditions. After the incubation, the cells were washed with 1× PBS and collected in RIPA buffer. Western blotting was performed using anti-puromycin antibody (Millipore, MABE343) as well as the following antibodies. Quantification of the western blots was conducted by normalizing the measured gene of interest to the respective loading control, with final values given as percentages of the respective control (DMSO) group. Quantification of the puromycin assay was performed using Ponceau-normalized signal intensities for the respective lanes, with the final values expressed as percentages of DMSO. Signal intensities were obtained using the image analysis software Fiji.

Antibodies used included anti-phospho p70 S6 kinase (Thr389) (Cell Signaling, 9206, 1:1,000); anti-phospho-4E-BP1 (Thr37/46) (Cell Signaling, 2855, 1:1,000); anti-MuRF (Abcam, 172479, 1:1,000); anti-vinculin (Abcam, 129002, 1:1,000); anti-4E-BP1 (Cell Signaling, 9644, 1:1,000); and anti-p70S6 kinase (Cell Signaling, 2708, 1:1,000). All antibodies were diluted in 3% BSA–TBST.

RNA isolation and quantitative RT–PCR. RNA was isolated using the RNeasy Mini kit (Qiagen, 74106) and reverse transcribed with the High-Capacity RNA-to-cDNA Kit (Thermo Fisher Scientific, 4387406). Gene expression was measured by qPCR using the Power SYBR Green Master Mix (Thermo Fisher Scientific, 4367659). All qPCR results were calculated relative to the mean of the housekeeping gene *Gapdh*. The average of two technical replicates was used for each biological data point. Primer sets for quantitative RT-PCR analyses are shown in Supplementary Table 2.

Immunocytochemistry. C2C12 cells cultured on a sterilized coverslip in six-well plates (Greiner Bio-One, CELLSTAR, 657160) were fixed in Fixx solution (Thermo Fisher Scientific, 9990244) for 15 min and permeabilized in 0.1% Triton X-100 (Amresco, 0694) solution for 15 min at 20 °C. Cells were blocked in 3% BSA for 1 h at 20 °C to avoid nonspecific antibody binding and then incubated with primary antibody overnight at 4 °C with gentle shaking. MyHC was stained for using the MF20 primary antibody (1:200, Invitrogen, 14-6503-82) for C2C12 cells and in Lonza muscle cells with an anti-MYL2 antibody (1:140, Abcam, ab79935). The next day, cells were incubated with secondary antibody (Thermo Fisher Scientific, A10037 for MF20 and A-21206 for MYL2) for 1 h at 20 °C, and nuclei were labeled with DAPI. The immunofluorescence images were acquired using either fluorescence or confocal microscopy. The myofusion index was calculated as the ratio of nuclei within myotubes to total nuclei. The myotube diameter was measured for eight myotubes per image using ImageJ. The myotube area was calculated as the total area covered by myotubes.

Human studies

Young versus old skeletal muscle microarrays. Gene expression analysis of young versus old human muscle biopsies was obtained from publicly available dataset GSE25941 (ref. [76]). Briefly, a total of 36 individuals were included in the study. The young (n = 15, 25 ± 1 y) participants included seven males and eight females. The older (n = 21, 78 ± 1 years) participants included 10 males and 11 females. All participants were healthy and had never been involved in any formal exercise. Skeletal muscle biopsies were obtained from the vastus lateralis in the basal state. The Affymetrix Human Genome U133 Plus 2.0 Array platform was used to perform the microarray analysis.

UK Biobank. We ran genetic association analyses for hand grip strength in UKBB participants 65 years of age or older (n = 93,211). These individuals were selected from the 379,530 unrelated individuals[49]. To determine the threshold for Bonferroni correction of multiple testing, we pruned the independent SNPs (r^2 < 0.1) within the *SPTLC1* region. We included SNPs with minor allele frequency > 0.1 within ± 150 kb of the human *SPTLC1* gene. As there were two effective independent SNPs for *SPTLC1*, we considered Bonferroni-corrected P < 0.025 significant. Nominal P values are reported in the text. For association analysis between genetic variants and hand grip strength, we used a linear regression model adjusting for sex, age and body mass index. The UKBB data were analyzed under the application 48020.

Helsinki Birth Cohort Study. The HBCS includes 13,345 individuals born in Helsinki between 1934 and 1944. The clinical study protocol was approved by the Ethics Committee of Epidemiology and Public Health of the Hospital District of Helsinki and Uusimaa. Written informed consent was obtained from each participant before any study procedure was initiated. The SFT describing the physical performance of the participants was performed to 695 individuals as previously

described[77] (Table 1). Here, we used a modified test battery, consisting of five components of the SFT: number of full arm stands in 30 s with arms folded across the chest to assess lower body strength, number of biceps curls in 30 s while holding a hand weight (3 kg for men and 2 kg for women) to assess upper body strength, chair sit and reach to assess lower body flexibility (from sitting position with leg extended at the front of the chair and hands reaching toward toes, distance (in cm) (plus/minus) from extended fingers to the tip of the toe), number of meters walked in 6 min to measure aerobic endurance and back scratch to assess upper body flexibility (with one hand reaching over the shoulder and the other one up the middle of the back, distance (in cm) between extended middle fingers (plus/minus)). The result of each test was expressed as age (for each 5-year group) and sex-standardized percentile scores. An overall test score was calculated by summarizing the normalized scores of the five SFT components. Isometric grip strength of the dominating hand was tested by a Newtest Grip Force dynamometer (Newtest Oy). The maximum value of three squeezes was used in the analyses of linear regression. Body mass index used in the analyses was collected at the time of grip strength measurements.

DNA was extracted from blood samples, and genotyping was performed with the modified Illumina 610k chip by the Wellcome Trust Sanger Institute, Cambridge, UK, according to standard protocols. Genomic coverage was extended by imputation using the 1000 Genomes Phase I integrated variant set (v3/April 2012; National Center for Biotechnology Information build 37 / hg19) as the reference sample and the IMPUTE2 software. Before imputation, the following QC filters were applied: SNP clustering probability for each genotype > 95%, call rate > 95% for individuals and markers (99% for markers with mirror allele frequency (MAF) < 5%), MAF > 1%, Hardy–Weinberg equilibrium $P > 1\times10^{-6}$. Moreover, heterozygosity, sex check and relatedness checks were performed and any discrepancies were removed.

For phenotype associations in the HBCS, the scores of the fitness tests were classified based on 5th percentile range, with a score of 1 being the worst performance (score below 5th percentile), 2 the score from the 5th to 9th percentile, and 20 the best performance (in or above the 95th percentile) as described[51]. To reduce confounding effects, individuals with diabetes were not included in the analyses. Otherwise, association analyses in HBCS were performed in individuals with genotype and SFT data available, approximately 400 individuals for the analysis. We performed linear regressions with R assuming an additive genetic model. We adjusted all models for age, sex, BMI, highest education achieved (basic or less, upper secondary, lower tertiary, upper tertiary) and smoking (yes or no). The SNPs were checked for potential other phenotypes at https://msk.hugeamp.org/.

Skeletal muscle gene expression in the GTEx Project. For RNA gene expression analyses, we used 706 postmortem skeletal muscle biopsies from the GTEx gene expression data collected as described[78]. As measures of gene expression, we used residual expression levels of transcripts adjusting for the published GTEx v8 covariates. As for expression quantitative trait locus analyses, we used the GTEx v8 genotypes (dbGaP, approved request #10143-AgingX).

Reporting summary

Further information on research design is available in the Nature Portfolio Reporting Summary linked to this article.

Data availability

RNA sequencing data are deposited in the GEO repository with the ID GSE213110. Experiments are depicted as single data points to enhance transparency. Experimental data are available upon reasonable request from the corresponding authors. Human clinical data from the HBCS cannot be shared due to data privacy. UKBB data are available from the public repository. Source data are provided with this paper.

References

1. Rowe, J. W. & Kahn, R. L. Successful aging. *Gerontologist* **37**, 433–440 (1997).
2. Bloom, D. E. et al. Macroeconomic implications of population ageing and selected policy responses. *Lancet* **385**, 649–657 (2015).
3. Johnston, M. C., Crilly, M., Black, C., Prescott, G. J. & Mercer, S. W. Defining and measuring multimorbidity: a systematic review of systematic reviews. *Eur. J. Public Health* **29**, 182–189 (2019).
4. Cruz-Jentoft, A. J. et al. Sarcopenia: revised European consensus on definition and diagnosis. *Age Ageing* **48**, 16–31 (2019).
5. Mitnitski, A. B., Mogilner, A. J. & Rockwood, K. Accumulation of deficits as a proxy measure of aging. *ScientificWorldJournal* **1**, 323–336 (2001).
6. Murton, A. J. & Greenhaff, P. L. Muscle atrophy in immobilization and senescence in humans. *Curr. Opin. Neurol.* **22**, 500–505 (2009).
7. Sousa-Victor, P. et al. Geriatric muscle stem cells switch reversible quiescence into senescence. *Nature* **506**, 316–321 (2014).
8. Sousa-Victor, P. & Munoz-Canoves, P. Regenerative decline of stem cells in sarcopenia. *Mol. Asp. Med.* **50**, 109–117 (2016).
9. Brack, A. S. & Munoz-Canoves, P. The ins and outs of muscle stem cell aging. *Skelet. Muscle* **6**, 1 (2016).
10. Larsson, L. et al. Sarcopenia: aging-related loss of muscle mass and function. *Physiol. Rev.* **99**, 427–511 (2019).
11. Giannoulis, M. G., Martin, F. C., Nair, K. S., Umpleby, A. M. & Sonksen, P. Hormone replacement therapy and physical function in healthy older men. Time to talk hormones? *Endocr. Rev.* **33**, 314–377 (2012).
12. Vetrano, D. L. et al. Frailty and multimorbidity: a systematic review and meta-analysis. *J. Gerontol. A Biol. Sci. Med. Sci.* **74**, 659–666 (2019).
13. Konig, M., Spira, D., Demuth, I., Steinhagen-Thiessen, E. & Norman, K. Polypharmacy as a risk factor for clinically relevant sarcopenia: results from the Berlin Aging Study II. *J. Gerontol. A Biol. Sci. Med. Sci.* **73**, 117–122 (2017).
14. Hannun, Y. A. & Obeid, L. M. Sphingolipids and their metabolism in physiology and disease. *Nat. Rev. Mol. Cell Biol.* **19**, 175–191 (2018).
15. Meikle, P. J. & Summers, S. A. Sphingolipids and phospholipids in insulin resistance and related metabolic disorders. *Nat. Rev. Endocrinol.* **13**, 79–91 (2017).
16. Havulinna, A. S. et al. Circulating ceramides predict cardiovascular outcomes in the population-based FINRISK 2002 Cohort. *Arterioscler. Thromb. Vasc. Biol.* **36**, 2424–2430 (2016).
17. Choi, S. & Snider, A. J. Sphingolipids in high fat diet and obesity-related diseases. *Mediators Inflamm.* **2015**, 520618 (2015).
18. Filippov, V. et al. Increased ceramide in brains with Alzheimer's and other neurodegenerative diseases. *J. Alzheimers Dis.* **29**, 537–547 (2012).
19. Laurila, P. P. et al. Inhibition of sphingolipid de novo synthesis counteracts muscular dystrophy. *Sci. Adv.* **8**, eabh4423 (2022).
20. Kurz, J., Parnham, M. J., Geisslinger, G. & Schiffmann, S. Ceramides as novel disease biomarkers. *Trends Mol. Med.* **25**, 20–32 (2019).
21. Summers, S. A. The ART of lowering ceramides. *Cell Metab.* **22**, 195–196 (2015).
22. Trayssac, M., Hannun, Y. A. & Obeid, L. M. Role of sphingolipids in senescence: implication in aging and age-related diseases. *J. Clin. Invest.* **128**, 2702–2712 (2018).
23. Hojjati, M. R. et al. Effect of myriocin on plasma sphingolipid metabolism and atherosclerosis in *apoE*-deficient mice. *J. Biol. Chem.* **280**, 10284–10289 (2005).
24. Ussher, J. R. et al. Inhibition of de novo ceramide synthesis reverses diet-induced insulin resistance and enhances whole-body oxygen consumption. *Diabetes* **59**, 2453–2464 (2010).

25. Zabielski, P. et al. The effect of high-fat diet and inhibition of ceramide production on insulin action in liver. *J. Cell. Physiol.* **234**, 1851–1861 (2019).
26. Turpin, S. M. et al. Obesity-induced CerS6-dependent C16:0 ceramide production promotes weight gain and glucose intolerance. *Cell Metab.* **20**, 678–686 (2014).
27. Hammerschmidt, P. et al. CerS6-derived sphingolipids interact with Mff and promote mitochondrial fragmentation in obesity. *Cell* **177**, 1536–1552 (2019).
28. Tosetti, B. et al. A tissue-specific screen of ceramide expression in aged mice identifies ceramide synthase-1 and ceramide synthase-5 as potential regulators of fiber size and strength in skeletal muscle. *Aging Cell* **19**, e13049 (2020).
29. Chaurasia, B. et al. Targeting a ceramide double bond improves insulin resistance and hepatic steatosis. *Science* **365**, 386–392 (2019).
30. De Larichaudy, J. et al. TNF-α- and tumor-induced skeletal muscle atrophy involves sphingolipid metabolism. *Skelet. Muscle* **2**, 2 (2012).
31. Turpin, S. M., Lancaster, G. I., Darby, I., Febbraio, M. A. & Watt, M. J. Apoptosis in skeletal muscle myotubes is induced by ceramides and is positively related to insulin resistance. *Am. J. Physiol. Endocrinol. Metab.* **291**, E1341–E1350 (2006).
32. Rivas, D. A. et al. Increased ceramide content and NFκB signaling may contribute to the attenuation of anabolic signaling after resistance exercise in aged males. *J. Appl. Physiol. (1985)* **113**, 1727–1736 (2012).
33. Turner, N. et al. A selective inhibitor of ceramide synthase 1 reveals a novel role in fat metabolism. *Nat. Commun.* **9**, 3165 (2018).
34. Pagadala, M., Kasumov, T., McCullough, A. J., Zein, N. N. & Kirwan, J. P. Role of ceramides in nonalcoholic fatty liver disease. *Trends Endocrinol. Metab.* **23**, 365–371 (2012).
35. Lone, M. A., Santos, T., Alecu, I., Silva, L. C. & Hornemann, T. 1-Deoxysphingolipids. *Biochim. Biophys. Acta, Mol. Cell. Biol. Lipids* **1864**, 512–521 (2019).
36. Andreux, P. A. et al. Systems genetics of metabolism: the use of the BXD murine reference panel for multiscalar integration of traits. *Cell* **150**, 1287–1299 (2012).
37. Brunner, F. et al. Effects of aging on type II muscle fibers: a systematic review of the literature. *J. Aging Phys. Act.* **15**, 336–348 (2007).
38. Wohlwend, M. et al. The exercise-induced long noncoding RNA CYTOR promotes fast-twitch myogenesis in aging. *Sci. Transl. Med.* **13**, eabc7367 (2021).
39. Mebarek, S. et al. Inhibition of de novo ceramide synthesis upregulates phospholipase D and enhances myogenic differentiation. *J. Cell Sci.* **120**, 407–416 (2007).
40. Cosgrove, B. D. et al. Rejuvenation of the muscle stem cell population restores strength to injured aged muscles. *Nat. Med.* **20**, 255–264 (2014).
41. Zhang, H. et al. NAD^+ repletion improves mitochondrial and stem cell function and enhances life span in mice. *Science* **352**, 1436–1443 (2016).
42. Adachi, R. et al. Pharmacological characterization of synthetic serine palmitoyltransferase inhibitors by biochemical and cellular analyses. *Biochem. Biophys. Res. Commun.* **497**, 1171–1176 (2018).
43. Kojima, T. et al. Discovery of novel serine palmitoyltransferase inhibitors as cancer therapeutic agents. *Bioorg. Med. Chem.* **26**, 2452–2465 (2018).
44. Siddique, M. M., Li, Y., Chaurasia, B., Kaddai, V. A. & Summers, S. A. Dihydroceramides: from bit players to lead actors. *J. Biol. Chem.* **290**, 15371–15379 (2015).
45. Xie, S. Z. et al. Sphingolipid modulation activates proteostasis programs to govern human hematopoietic stem cell self-renewal. *Cell Stem Cell* **25**, 639–653 (2019).
46. Sukumaran, P. et al. Complexation of C6-ceramide with cholesteryl phosphocholine—a potent solvent-free ceramide delivery formulation for cells in culture. *PLoS ONE* **8**, e61290 (2013).
47. Holliday, M. W. Jr., Cox, S. B., Kang, M. H. & Maurer, B. J. C22:0- and C24:0-dihydroceramides confer mixed cytotoxicity in T-cell acute lymphoblastic leukemia cell lines. *PLoS ONE* **8**, e74768 (2013).
48. Bohannon, R. W. Grip strength: an indispensable biomarker for older adults. *Clin. Interv. Aging* **14**, 1681–1691 (2019).
49. Bycroft, C. et al. The UK Biobank resource with deep phenotyping and genomic data. *Nature* **562**, 203–209 (2018).
50. Felicio, D. C. et al. Poor correlation between handgrip strength and isokinetic performance of knee flexor and extensor muscles in community-dwelling elderly women. *Geriatr. Gerontol. Int.* **14**, 185–189 (2014).
51. Eriksson, J. G. et al. Prenatal and childhood growth and physical performance in old age—findings from the Helsinki Birth Cohort Study 1934–1944. *Age* **37**, 108 (2015).
52. ENCODE Project Consortium et al. Expanded encyclopaedias of DNA elements in the human and mouse genomes. *Nature* **583**, 699–710 (2020).
53. Trierweiler, H. et al. Sarcopenia: a chronic complication of type 2 diabetes mellitus. *Diabetol. Metab. Syndr.* **10**, 25 (2018).
54. Bieberich, E. Ceramide in stem cell differentiation and embryo development: novel functions of a topological cell-signaling lipid and the concept of ceramide compartments. *J. Lipids* **2011**, 610306 (2011).
55. Borsch, A. et al. Molecular and phenotypic analysis of rodent models reveals conserved and species-specific modulators of human sarcopenia. *Commun. Biol.* **4**, 194 (2021).
56. Sogaard, D. et al. Muscle-saturated bioactive lipids are increased with aging and influenced by high-intensity interval training. *Int. J. Mol. Sci.* https://doi.org/10.3390/ijms20051240 (2019).
57. Balage, M. et al. Presence of low-grade inflammation impaired postprandial stimulation of muscle protein synthesis in old rats. *J. Nutr. Biochem.* **21**, 325–331 (2010).
58. Argiles, J. M., Busquets, S., Stemmler, B. & Lopez-Soriano, F. J. Cachexia and sarcopenia: mechanisms and potential targets for intervention. *Curr. Opin. Pharmacol.* **22**, 100–106 (2015).
59. Chen, Z., Li, B., Zhan, R. Z., Rao, L. & Bursac, N. Exercise mimetics and JAK inhibition attenuate IFN-γ-induced wasting in engineered human skeletal muscle. *Sci. Adv.* https://doi.org/10.1126/sciadv.abd9502 (2021).
60. Haider, S. I., Johnell, K., Weitoft, G. R., Thorslund, M. & Fastbom, J. The influence of educational level on polypharmacy and inappropriate drug use: a register-based study of more than 600,000 older people. *J. Am. Geriatr. Soc.* **57**, 62–69 (2009).
61. Carroll, J. One drug, many uses. *Biotechnol. Healthc.* **2**, 56–61 (2005).
62. Matyash, V., Liebisch, G., Kurzchalia, T. V., Shevchenko, A. & Schwudke, D. Lipid extraction by methyl-tert-butyl ether for high-throughput lipidomics. *J. Lipid Res.* **49**, 1137–1146 (2008).
63. Knittelfelder, O. L., Weberhofer, B. P., Eichmann, T. O., Kohlwein, S. D. & Rechberger, G. N. A versatile ultra-high performance LC-MS method for lipid profiling. J. Chromatogr. B Analyt. Technol. Biomed. *Life. Sci.* **951-952**, 119–128 (2014).
64. Othman, A. et al. Plasma deoxysphingolipids: a novel class of biomarkers for the metabolic syndrome? *Diabetologia* **55**, 421–431 (2012).
65. Checa, A. et al. Hexosylceramides as intrathecal markers of worsening disability in multiple sclerosis. *Mult. Scler.* **21**, 1271–1279 (2015).
66. Pirinen, E. et al. Pharmacological inhibition of poly(ADP-ribose) polymerases improves fitness and mitochondrial function in skeletal muscle. *Cell Metab.* **19**, 1034–1041 (2014).

67. Shiotsuki, H. et al. A rotarod test for evaluation of motor skill learning. *J. Neurosci. Methods* **189**, 180–185 (2010).
68. von Euler, M. et al. Inhalation of low concentrations of toluene induces persistent effects on a learning retention task, beam-walk performance, and cerebrocortical size in the rat. *Exp. Neurol.* **163**, 1–8 (2000).
69. Zanou, N. et al. Role of TRPC1 channel in skeletal muscle function. *Am. J. Physiol. Cell. Physiol.* **298**, C149–C162 (2010).
70. Luan, P. et al. Urolithin A improves muscle function by inducing mitophagy in muscular dystrophy. *Sci. Transl. Med.* https://doi.org/10.1126/scitranslmed.abb0319 (2021).
71. Brooks, S. V. & Faulkner, J. A. Contractile properties of skeletal muscles from young, adult and aged mice. *J. Physiol.* **404**, 71–82 (1988).
72. Law, C. W., Chen, Y., Shi, W. & Smyth, G. K. voom: precision weights unlock linear model analysis tools for RNA-seq read counts. *Genome Biol.* **15**, R29 (2014).
73. Kolmert, J. et al. Lipid mediator quantification in isolated human and guinea pig airways: an expanded approach for respiratory research. *Anal. Chem.* **90**, 10239–10248 (2018).
74. Campisi, G. M. et al. Determination of the serine palmitoyl transferase inhibitor myriocin by electrospray and Q-trap mass spectrometry. *Biomed. Chromatogr.* https://doi.org/10.1002/bmc.4026 (2017).
75. Sanjana, N. E., Shalem, O. & Zhang, F. Improved vectors and genome-wide libraries for CRISPR screening. *Nat. Methods* **11**, 783–784 (2014).
76. Raue, U. et al. Transcriptome signature of resistance exercise adaptations: mixed muscle and fiber type specific profiles in young and old adults. *J. Appl. Physiol.* **112**, 1625–1636 (2012).
77. Jantunen, H. et al. Objectively measured physical activity and physical performance in old age. *Age Ageing* **46**, 232–237 (2017).
78. GTEx Consortium. The Genotype-Tissue Expression (GTEx) pilot analysis: multitissue gene regulation in humans. *Science* **348**, 648–660 (2015).
79. Subramanian, A. et al. Gene set enrichment analysis: a knowledge-based approach for interpreting genome-wide expression profiles. *Proc. Natl Acad. Sci. USA* **102**, 15545–15550 (2005).

Acknowledgements

We wish to thank the staff of the Ecole Polytechnique Federale de Lausanne (EPFL) histology, flow cytometry and animal facilities for technical assistance. J. Tuhkanen is thanked for data management with the HBCS. We also wish to acknowledge T. Teav (from the Metabolomics Platform at UNIL) for his help with sphingolipid measurement. The work in the laboratory of J.A. was supported by grants from the EPFL, the European Research Council (ERC-AdG-787702), the Swiss National Science Foundation (SNSF 31003A_179435), the Fondation Suisse de Recherche sur les Maladies Musculaires (FSRMM) and the Fondation Marcel Levaillant (190917). We thank all study participants as well as everybody involved in the HBCS. The work has been supported by the Academy of Finland, the Finnish Diabetes Research Society, the Folkhälsan Research Foundation, the Novo Nordisk Foundation, Finska Läkaresällskapet, the Finnish Foundation for Cardiovascular Research, the Juho Vainio Foundation, the Signe and Ane Gyllenberg Foundation, the University of Helsinki, the Sigrid Juselius Foundation, the Ministry of Education, the Ahokas Foundation, the Emil Aaltonen Foundation, the Paavo Nurmi Foundation, the Orion Foundation and a Scottish Senior Clinical Fellowship (SCD/09). We would also like to acknowledge the Genetics Core of the Wellcome Trust Clinical Research Facility (Edinburgh, UK) who ran the 450k array for the HBCS samples. P.-P.L. was a recipient of a Sigrid Juselius Fellowship. This research has been conducted using the UKBB resource.

Author contributions

The study was conceived and designed by P.-P.L. and J.A. Human and mouse bioinformatics analyses were performed by P.P.L. Mouse phenotyping was carried out by P.-P.L. and N.Z. RNA sequencing was analyzed by M.B.-S. and P.-P.L. In vitro work was performed by M.W., T.I.L., S.H., P.-P.L. and D.D.A. H.G.-A., T.O.E., M.K.H., and J.I. performed sphingolipid measurements. Histological analyses, ex vivo measurements and MuSC extractions and injections were performed by P.L. Genetic analyses were performed by P.-P.L., E.P. and J.L. Human data were collected by M.S. and J.G.E. P.-P.L. and J.A. wrote the manuscript, and all authors gave critical comments on it. Z.K., N.P., C.M. and J.A. supervised the work.

Competing interests

P.-P.L. and J.A. are inventors on a provisional patent application from the EPFL related to the role of sphingolipids on muscle function. The remaining authors declare no competing interests.

Additional information

Supplementary information The online version contains supplementary material available at https://doi.org/10.1038/s43587-022-00309-6.

Correspondence and requests for materials should be addressed to Pirkka-Pekka Laurila or Johan Auwerx.

Peer review information *Nature Aging* thanks Yusuf Hannun, Joris Deelen, and the other, anonymous, reviewer(s) for their contribution to the peer review of this work.

nature portfolio

Corresponding author(s): Johan Auwerx, Pirkka-Pekka Laurila

Last updated by author(s): 2022/07/07

Reporting Summary

Nature Portfolio wishes to improve the reproducibility of the work that we publish. This form provides structure for consistency and transparency in reporting. For further information on Nature Portfolio policies, see our Editorial Policies and the Editorial Policy Checklist.

Statistics

For all statistical analyses, confirm that the following items are present in the figure legend, table legend, main text, or Methods section.

n/a	Confirmed	
☐	☒	The exact sample size (*n*) for each experimental group/condition, given as a discrete number and unit of measurement
☐	☒	A statement on whether measurements were taken from distinct samples or whether the same sample was measured repeatedly
☐	☒	The statistical test(s) used AND whether they are one- or two-sided *Only common tests should be described solely by name; describe more complex techniques in the Methods section.*
☐	☒	A description of all covariates tested
☐	☒	A description of any assumptions or corrections, such as tests of normality and adjustment for multiple comparisons
☐	☒	A full description of the statistical parameters including central tendency (e.g. means) or other basic estimates (e.g. regression coefficient) AND variation (e.g. standard deviation) or associated estimates of uncertainty (e.g. confidence intervals)
☐	☒	For null hypothesis testing, the test statistic (e.g. *F*, *t*, *r*) with confidence intervals, effect sizes, degrees of freedom and *P* value noted *Give P values as exact values whenever suitable.*
☒	☐	For Bayesian analysis, information on the choice of priors and Markov chain Monte Carlo settings
☒	☐	For hierarchical and complex designs, identification of the appropriate level for tests and full reporting of outcomes
☐	☒	Estimates of effect sizes (e.g. Cohen's *d*, Pearson's *r*), indicating how they were calculated

Our web collection on statistics for biologists contains articles on many of the points above.

Software and code

Policy information about availability of computer code

Data collection	Standard R packages were used.
Data analysis	Standard R packages were used.

For manuscripts utilizing custom algorithms or software that are central to the research but not yet described in published literature, software must be made available to editors and reviewers. We strongly encourage code deposition in a community repository (e.g. GitHub). See the Nature Portfolio guidelines for submitting code & software for further information.

Data

Policy information about availability of data

All manuscripts must include a data availability statement. This statement should provide the following information, where applicable:

- Accession codes, unique identifiers, or web links for publicly available datasets
- A description of any restrictions on data availability
- For clinical datasets or third party data, please ensure that the statement adheres to our policy

RNA sequencing data will be provided in public repository upon publication.

Human research participants

Policy information about studies involving human research participants and Sex and Gender in Research.

Reporting on sex and gender	Human genetic analyses were adjusted for sex. Both sexes were included.
Population characteristics	Statistical analysis of the genetic cohorts has been described in the methods. Standard methods were used.
Recruitment	This study is based on existing cohorts.
Ethics oversight	The HBCS was approved by the Ethical Committee of the University of Helsinki.

Note that full information on the approval of the study protocol must also be provided in the manuscript.

Field-specific reporting

Please select the one below that is the best fit for your research. If you are not sure, read the appropriate sections before making your selection.

☒ Life sciences ☐ Behavioural & social sciences ☐ Ecological, evolutionary & environmental sciences

For a reference copy of the document with all sections, see nature.com/documents/nr-reporting-summary-flat.pdf

Life sciences study design

All studies must disclose on these points even when the disclosure is negative.

Sample size	Sample sizes were chosen based on studies with similar experimental design and on the known variability of the assay
Data exclusions	Mice that showed signs of severity, predefined by the animal authorizations, were euthanized. No other data was excluded.
Replication	All attempts to reproduce data were successful. Genetic knockouts of the sphingolipid pathway reproduced findings of pharmagological inhibition in both mice and in cells. Standard methods were used in replication for human genetic findinds.
Randomization	For all the animal experiments mice were randomly allocated to distinct groups based on body weight.
Blinding	Sacrifice of the mice was blinded by the staff, and animals coded with a running number. Grip strength and beam walk tests were performed blinded. To control for variance of different lanes in treadmill and rotarod tests, mice of only one group were run simultaneously on a treadmill or rotarod.

Reporting for specific materials, systems and methods

We require information from authors about some types of materials, experimental systems and methods used in many studies. Here, indicate whether each material, system or method listed is relevant to your study. If you are not sure if a list item applies to your research, read the appropriate section before selecting a response.

Materials & experimental systems

n/a	Involved in the study
☐	☒ Antibodies
☐	☒ Eukaryotic cell lines
☒	☐ Palaeontology and archaeology
☐	☒ Animals and other organisms
☒	☐ Clinical data
☒	☐ Dual use research of concern

Methods

n/a	Involved in the study
☒	☐ ChIP-seq
☒	☐ Flow cytometry
☒	☐ MRI-based neuroimaging

Antibodies

Antibodies used	A list of antibodies is provided.
Validation	Antibodies of the study are widely used, and their detailed identifications are provided in the list of antibodies used.

Eukaryotic cell lines

Policy information about cell lines and Sex and Gender in Research

Cell line source(s)	Stated in Cell culture and cell transfection.
Authentication	Commonly used cell lines
Mycoplasma contamination	Negative for mycoplasma contamination. Stated in Cell culture and cell transfection
Commonly misidentified lines (See ICLAC register)	N/A

Animals and other research organisms

Policy information about studies involving animals; ARRIVE guidelines recommended for reporting animal research, and Sex and Gender in Research

Laboratory animals	Methods: Animals.
Wild animals	Study did not involve wild animals.
Reporting on sex	This study was conducted in male mice. Such an approach allows controlling for variance in sex. The human validation included both male and female participants.
Field-collected samples	Did not involve field-collected samples.
Ethics oversight	Animal protocols were approved by the Canton of Vaud, Switzerland.

Note that full information on the approval of the study protocol must also be provided in the manuscript.